Role of clustered protocadherin-γ in PV-positive neurons for the formation of cortical neuronal circuit

大脳皮質神経回路形成における PV 陽性細胞のクラスター型プロトカドヘリンの役割

2022 年 3 月

大阪大学生命機能研究科

河村菜々実

ABSTRACT

In the cortex, functional neural circuits are formed by specific neural connections between many types of inhibitory and excitatory neurons. However, the molecular mechanisms for the recognition of synaptic partners have remained unclear. I focused on clustered protocadherin (cPcdh) which is a diversified membrane adhesion molecule as a candidate for the recognition molecules between neurons. cPcdh consists of 58 isoforms which are divided into three gene cluster structures (α, β, and γ) in its genome and they have homophilic adhesion properties. In the CNS, cPcdhs are expressed in most neurons. Around 15 isoforms are stochastically expressed in different combinations in each cell, which gives each cell its individuality. It has been reported that the deletion of cPcdhγ in inhibitory neurons in the telencephalic region, abnormal long-lasting neural activity had been observed by whisker stimulation in the somatosensory cortex. These results suggest that cPcdhγ in inhibitory neurons could be involved in the formation of appropriate cortical neural circuits. A variety of inhibitory neurons exist in the cerebral cortex. Among them, parvalbumin-expressing (PV^+) neuron occupies 50% of the inhibitory neural population and high frequently forms reciprocal connections with pyramidal neurons. It is thought to play important roles in information processing by modulation of visual response property of pyramidal cells and generation of the cortical gamma oscillation. In this study, I investigated the influence of cPcdhγ deletion in PV^+ neurons on local neural circuits that form with PV^+ neurons and pyramidal neurons in the primary visual cortex of mice by whole-cell patch clamp recording in conditional cPcdhγ deletion mice in PV^+ neuron (*PV-Cre; cPcdhγ$^{fl/fl}$*: KO mice). The deletion of cPcdhγ in PV^+ neurons did not affect the membrane properties of PV^+ neurons and pyramidal neurons. To examine the connection between PV^+ neurons and pyramidal neurons, simultaneous double whole-cell recordings were performed. The connection probability between PV^+ neuron and pyramidal neurons and the strength of unitary inhibitory synaptic responses were similar between control and KO mice. I examined the connection relationship between PV^+ and multiple neighboring pyramidal neurons in control mice by multiple whole-cell recordings. As a result, I found two types of PV^+ neurons with different connectivity with pyramidal neurons: high reciprocal connectivity to neighboring pyramidal neurons (high-reciprocity) and low-reciprocity. Surprisingly, those classifications were lost in KO mice, indicating that cPcdhγ might determine the differential connectivity of each PV^+ neuron within layer 2/3. To reveal the influence of cPcdhγ KO in interlaminar connectivity, I performed excitatory input map through layer 2/3 to layer 6 by whole-cell recording and laser-scan photostimulation using caged glutamate. I found that cPcdhγ-deleted PV^+ neurons receive more inputs from layer 5 and layer 6 pyramidal cells compared to control mice. These results indicate that cPcdhγ is involved in not only intralaminar connections but also interlaminar connections in the visual cortex. To investigate the relationship between expression patterns of cPcdhγ isoforms in each neuron and neural connectivity, I combined whole-cell patch

clamp with single cell RNA sequence. I found that reciprocally connected PV^+ neurons and pyramidal neurons shared the same type of cPcdhγ isoforms significantly more compared to shuffled data. This study revealed that cPcdhγ PV^+ neurons regulate the specificity of cortical intralaminar and interlaminar networks.

INDEX

GENERAL INTRODUCTION

All our consciousness and behavior are generated by the coordinated activity of a vast number of different neurons in the brain. The visual, tactile, auditory, olfactory, and gustatory information we receive is converted into electrical information by cells that have sensors to detect each of these factors, with changes in the membrane potential of the cells. Neurons transmit electrical information to other cells through synapses, which are connections between neurons. Interestingly, each neuron has its own threshold. No matter how much information is input from other neurons, if it does not exceed the threshold of the receiving neuron, the neuron will not be able to transmit the information to the next neuron. In order for neurons to transmit information, they need excitatory inputs that exceed a threshold. There are also some neuron types that transmit inhibitory inputs that suppress the activity of the connecting neurons when the activity threshold is exceeded (inhibitory neurons). These various neurons connect to each other in a non-random network to allow for the proper processing of information and the generation of higher-order functions such as cognition and learning. Thus, the balance between excitatory and inhibitory neurons (E-I balance) is very important for information processing in the cerebral cortex, and specific synaptic connections are essential for regulating this balance. In fact, it has been shown that the disruption of this E-I balance causes cognitive dysfunction such as schizophrenia (Yizhar et al., 2011). Thus, despite the critical role that synaptic connectivity plays in brain function, the mechanisms that determine its specificity remain unknown.

Clustered protocadherin

In this study, I focused on clustered protocadherin (cPcdh), which is a membrane protein with specific cell adhesion activity. *cPcdh* consists of three gene clusters, alpha, beta, and gamma, with 14, 22, and 22 isoforms in each cluster, and particularly strongly expressed in neurons (Kohmura et al.,1998; Wu et al., 1999; Yagi & Takeichi, 2000; Wu et al., 2001). There is a promoter region in front of each isoform sequence, and different combinations of *cPcdh* are expressed in each neuron to the stochastic selection of diverse variable regions in each cell, which gives the cell its individuality (Tasic et al., 2002; Wang et al., 2002; Kaneko et al., 2006). More interestingly, the cPcdh protein forms a cis-dimer and has specific trans-homophilic adhesion activity in the extracellular region (Schreiner & Weiner, 2010). In culture experiments, among the five cPcdh isoforms expressed, if one of them does not match, cell-cell aggregation does not occur. It is indicating that cPcdh has a highly specific adhesive activity. (Thu et al., 2014).

In addition, it has been reported that cPcdh interacts with the synaptogenic factors neuroligin-1 and neuroligin-2, respectively (Molumby et al., 2017; Steffen et al., 2021). Neuroligin is a post-

synaptic single transmembrane protein that regulates synaptic maturation and function by interacting with presynaptic Neurexin (Südhof, T. C., 2008). Experiments in cultured cells have shown that cPcdhγ blocks the Neuroligin-Neurexin interaction by interacting with Neuroligin (Molumby et al., 2017; Steffen et al., 2021). These results suggest that cPcdh has a role in determining the synaptic partner. The first results to support this hypothesis were shown in the somatosensory cortex of mice. In the cortex, clonal excitatory neuron pairs that differentiated from the same stem cell have been significantly higher rates of reciprocally connection pattern in which they are connected to each other than non-clonal cell pairs (Yu et al., 2009; Yu et al., 2012). However, specific reciprocal neural connections were lost in differentiation from stem cells that lacked all cPcdh (Tarusawa et al., 2016). This suggests that cPcdh is involved in the specificity of synaptic connections, recognizing and binding to the same clonal excitatory neurons.

cPcdh is also expressed in inhibitory neurons. In particular, deletion of *Emx*-specific cPcdhγ, a molecular marker expressed in excitatory neurons in the telencephalon, results in survival of the animal, whereas deletion of *Dlx*-specific cPcdhγ, an inhibitory neuronal marker, results in a phenotype of death within 30 days (Carriere et al., 2020; Ariga, in preparation). It has also been reported that in mice deleted for cPcdhα and β, the other two cPcdh clusters, animals survive (Leon et al., 2020). This suggests that among the three clusters of cPcdh, cPcdhγ, in particular, plays a critical role in inhibitory neurons.

In addition, at the age of 14-16 days, it was found that disrupted E-I balance, which excitability was not suppressed for a long time by whisker stimulation in the primary somatosensory cortex of *Dlx*-specific cPcdhγ deletion mice (Ariga, in preparation), it was later reported that this was caused by the inhibitory neuron death (Southwell et al., 2012; Wong et al., 2018). These results suggest that cPcdhγ could be involved in the formation of excitatory-inhibitory neuronal circuits in inhibitory neurons. However, since the deletion of *Dlx*-specific cPcdhγ causes cell death as described above, it has not been clarified what role cPcdhγ deletion has in neural circuits.

Expression analysis of cPcdh in single cells

cPcdh expression in a single cell was first revealed in cerebellar Purkinje cells (Esumi S et al., 2005). In this study, primers with specific sequences for each cPcdh isoform were designed and polymerase chain reaction (PCR) was performed to determine whether each isoform was expressed or not. However, in that study, it is unclear whether undetected isoforms were not expressed in cells, or the detection sensitivity of PCR is limited. Therefore, they further divided the reverse transcript of a single Purkinje cell into three samples, performed the same experiment, and confirmed that all three samples showed the same detection results. However, neurons in the cerebral cortex have smaller cell bodies and less *cPcdh* expression than Purkinje cells, even though the same experiment

was performed, the results of the three samples were mostly inconsistent, so the expression of *cPcdh* was not clarified. Thus, to confirm the expression of cPcdh in single neurons in the cerebral cortex, a new approach for full-length single-cell total RNA sequencing, RamDA-seq, was recently performed (Masuda, in preparation). Furthermore, RamDA-seq combined with whole-cell patch recording revealed that expression isoforms tended to significantly match in clonal excitatory neuron pairs compared to non-clonal cell pairs in the mouse somatosensory cortex. This is the first experiment that approaches the understanding of the relationship between cPcdh expression and local circuits. However, it is still unclear whether there is a difference in the tendency of expression of cPcdh isoform in different cell types.

Parvalbumin positive neurons

Inhibitory neurons in the cerebral cortex are known to consist of a variety of cell types, and different cell types have different roles in neural circuits (Burkhalter, 2008; Markram et al., 2004). Among them, parvalbumin-positive (PV^+) neurons are a major type of inhibitory neuron (Celio, 1986; Gonchar and Burkhalter, 1997; Kawaguchi & Kubota, 1997). Unlike other inhibitory neuronal types, PV^+ neurons have a characteristic fast-spiking firing pattern and synapse with the proximal dendrites and cell bodies of their target excitatory neurons. This is thought to provide strong inhibition to target cells and also regulate the timing of firing (DeFelipe, 1997; DeFelipe et al., 1999; Kisvárday & Eysel, 1993; Markram et al., 2004). PV^+ neurons are also involved in the regulation of responses to visual stimuli (Atallah et al., 2011) and the formation of gamma waves (Atallah et al., 2011), which are associated with memory information and sensory processing, thus, they are thought to play an important role in local neural circuits. PV^+ neurons are classified into chandelier cells and basket cells according to their morphology (Kubota et al., 2016). In recent years, single-cell RNA sequencing and other methods have further classified cell types (Gouwens et al., 2019). However, the functional differences between them remain unknown.

The layered structure of the cerebral cortex

Most areas of the cerebral cortex have a six-layered structure, with the thickness of the layers differing among cortical regions. Layer 1 is the most superficial layer, the molecular layer. It is composed mainly of neural fibers and dendrites. The terminal branches of the apical dendrites of pyramidal (Pyr) neurons in layers 2, 3, and 5 spread out this layer and form numerous synapses with projection fibers from the thalamus and with association and commissure fibers that communicate between the cortices. Layer 2 is the outer granule layer, consisting of granule cells and small Pyr neuron bodies. Layer 3 is the external pyramidal layer, consisting of medium-sized Pyr neuron bodies. In mice, the boundary between these two layers is difficult to identify and is

often grouped together as layer 2/3. The neurons in layer 2/3 output to the ipsilateral and contralateral cortex, and intercortical connections are the main source of information. Layer 4 is the inner granular layer, which consists of small stellate cells and is the main input layer from the thalamus. Layer 5 is the internal pyramidal layer, which consists of large Pyr neurons and is the output layer to the subcortical nucleus. Layer 5 in the visual cortex projects to the colliculus superior (Corticotectal fibres). The most inner of the layer structure is layer 6, which is the polymorphic cell layer. The most inner of the layer structure is layer 6, which is the multiform cell layer. Consisting of spindle cells of various shapes and sizes, neurons in this layer project axons to the thalamus (Shipp, S., 2007).

Primary visual cortex and local neural circuits

Many studies of cell-to-cell connections have been reported, mainly in the primary sensory areas of the cerebral cortex. The primary visual cortex (V1) is one of the most studied areas. The visual information received by the photoreceptor cells is projected to the contralateral thalamus and then to V1. V1 processes the simplest visual information, and excitatory neurons in that area have specific property called orientation selectivity, which is the ability of each cell to respond only to line segments of a specific orientation. Thus, this area has been the focus of much research as a region where it is easy to associate local neural circuits with their functional meaning. Many studies have been reported on the connection specificity between excitatory neurons, such as the clonality of cells, differences in orientation selectivity, and developmental stages (Yu et al., 2009; Yu et al., 2012; Ko et al., 2013; Ishikawa et al., 2014), however, there are few reports on the connection specificity between excitatory and inhibitory neurons. In layer 2/3 of the rat visual cortex, when there is a reciprocal connection between Pyr neurons which are excitatory neurons and PV^+ neurons, there is a specific microcircuit in which excitatory neurons in layers 2/3 and 4 form excitatory synaptic connections with both neurons (Yoshimura & Callaway, 2005). Moreover, it is reported that PV^+-Pyr neuron pairs just below the projection area from the lateral geniculate nucleus (LGN) of the thalamus to layer 1 have specificities according to their histological distribution, such as the amplitude of inhibitory input that Pyr neurons receive from PV^+ neurons, although the specificity of the connection probability remains the same (D'Souza et al., 2019).

There is also input specificity not only within intralaminar but also interlaminar. For example, neurons in layer 4 are mainly input to layer 2/3 but also input to layer 6. It has been shown that layer 2/3 neurons project information mainly to the higher cortex, while layer 6 neurons output to the LGN. This reveals the existence of a loop structure across the layers (Shipp, S., 2007; Briggs, F., 2010). Furthermore, in confirming circuits on a cell-to-cell scale, it was reported that the fine-scale neural circuits found in layers 2/3 and 4 could not be confirmed between layers 2/3 and 5

(Yoshimura & Callaway, 2005). This suggests that there are specific rules not only in the intralaminar but also between specific neuronal cell types between interlaminar. However, there have been few studies of such cell-scale local circuits between layers, and it is not clear how much cell-type specificity exists.

In this study, I focused on the local neural circuits between Pyr neurons and PV^+ neurons in the primary visual cortex of mice, and to clarify the role of cPcdhγ, I conducted experiments.

INTRODUCTION

Our consciousness and behavior are thought to be generated through the complex neural networks of the brain. However, it is still unclear how the specificity of neural circuits is regulated. reciprocal connections formed between two cells are the smallest units of local neural circuits. They exist in various regions of the brain, including the cerebral cortex and hippocampus, and are important closed circuits that generate sequential neural activity important for behavior, short-term memory, and decision-making. It is important to understand the specificity and mechanism of the binding between these two cells. c*Pcdh* has three gene cluster structures on the genome, and a total of 58 isoforms are expressed in different combinations in individual cells, which are thought to give cells their individuality. The same isoform of *cPcdh* has homophilic adhesive activity with each other, and it has been focused on as a factor in the formation of specific neural connections (Kaneko R et al., 2006). In a previous study, to examine the functional role of cPcdh in inhibitory neurons, generated mice that specifically deleted *cPcdhγ* in inhibitory neurons of the telencephalic region. The mice died by 3 weeks of age and showed long-lasting abnormalities of neural activity in the cortical somatosensory cortex in response to whisker stimulation (Ariga, in preparation). These results suggest that cPcdhγ could be involved in the formation of inhibitory neuronal circuits. In the primary visual cortex of rats, local neural circuits that depend on reciprocal connection between PV^+ neurons, a type of inhibitory neuron, and excitatory neurons are already known. To test whether cPcdhγ is involved in that specific neural circuit, I crossed mice that deleted cPcdhγ only PV^+ neurons, and analyzed their neural connectivity.

RESULTS

Chapter 1

Investigation of the effects induced by PV^{+} neurons specific cPcdhγ KO.

Morphological characteristics of PV^{+} neuron-specific *cPcdhγ* conditional knockout mice.

Deletion of *cPcdhγ* whole body from embryonic stage results in neonatal death from dramatic neurodegeneration. (Wang et al., 2002). Inhibitory neuron-specific deletion of *cPcdhγ* from embryonic development results in inhibitory neuronal death and growth-retardation (Ariga, in preparation; Carriere et al., 2020; Leon et al., 2020). To understand the role of cPcdhγ in PV^{+} neurons, I used *cPcdhγflox*$^{PV\text{-}Cre}$ mice (KO mice, see methods). First, I confirmed whether the PV^{+} neurons specific cPcdhγ deletion that is expressed after the embryonic stage causes developmental abnormalities in the mice. In mature mice, there was no significant difference in body weight between control and KO mice (Fig1). In addition, it has previously been reported that mice specifically deleted cPcdhγ in PV^{+} neurons do not show cell death (Carriere et al., 2020).

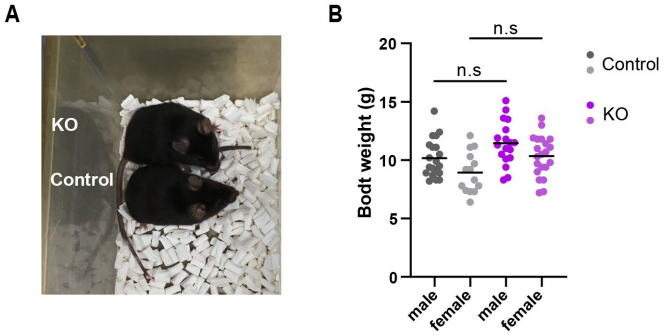

Fig. 1. PV^{+} neuron-specific *cPcdhγ* KO mice showed normal development.

(A) Adult male mouse at four months old. The upper one is KO mouse (*cPcdhgflox*$^{PV\text{-}Cre}$) and the lower one is control mouse(*cPcdhgflox*). (B) Bodyweight distribution by sex in mice at postnatal 21-26. One-way ANOVA Dunnett's T3 multiple comparisons test. Mean are shown; p=0.2403 (control male versus control female), p=0.3317 (KO male versus KO female), p=0.1772 (control male versus KO male), p=0.1410 (control female versus KO female), p=0.9996 (control male versus KO female), p=0.0030 (control female versus KO male).

Electrophysiological properties of PV$^+$ neuron-specific *cPcdhγ* conditional knockout mice.

Next, I tested the electrophysiological properties of PV$^+$ neurons to the effect of cPcdhγ deletion (Fig2). I conducted whole-cell recordings from PV$^+$ neurons that visualized by tdTomato is in layer 2/3 of the V1 field in postnatal 21-26 mice (Fig2A). I recorded and compared several membrane properties of KO mice, but found no significant difference between with control mice.

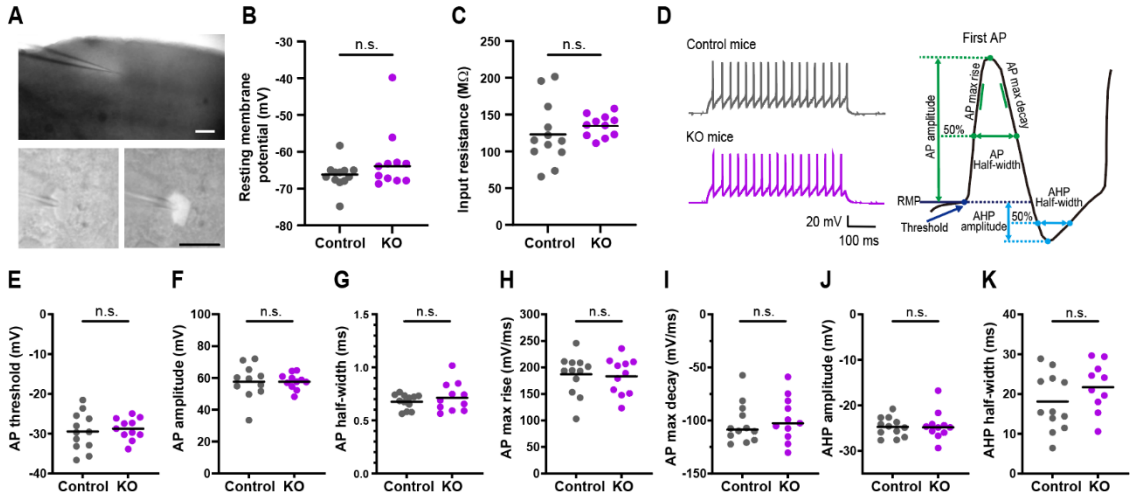

Fig. 2. PV$^+$ neuron-specific *cPcdhγ* KO does not affect the membrane properties of PV$^+$ neurons.
(A) Differential interference contrast image of a brain slice with recording electrode in a layer 2/3 V1(top). Scale bars, 200mm. High magnification images of tdTomato-positive cells in layer 2/3(bottom). Scale bars, 20mm. (B-C) The value of resting membrane potential (B), input resistance (C). (D) Representative traces of firing patterns of first action potentials (AP) evoked by depolarizing current injection (200 pA) in current clamp mode in PV$^+$ neurons from control mice (upper) and KO mice (bottom). Schematic representation of AP and each parameter measurement (right). (E-K) The value of AP threshold (E), AP amplitude (F), AP half-width (G), AP max rise (H), AP max decay (I), afterhyperpolarization (AHP) amplitude (J), AHP half-width (K). A bar indicates the median. Mann–Whitney U test, p=0.2534 (B), p=0.5658 (I), p=0.9887 (J). A bar indicates the mean. Welch's t test, p=0.4243 (C), p=0.6514 (E), p=0.9769 (F), p=0.3953 (G), p=0.8473 (H), p=0.1705 (K). control, n=10 mice: KO, n=9mice. n.s., not significant.

In addition, to reveal whether *cPcdhγ* KO is influencing the membrane properties of excitatory neurons, I recorded from pyramidal (Pyr) neurons that the major excitatory neuron in V1 (Fig3). The membrane property of Pyr neurons was normal in KO mice.

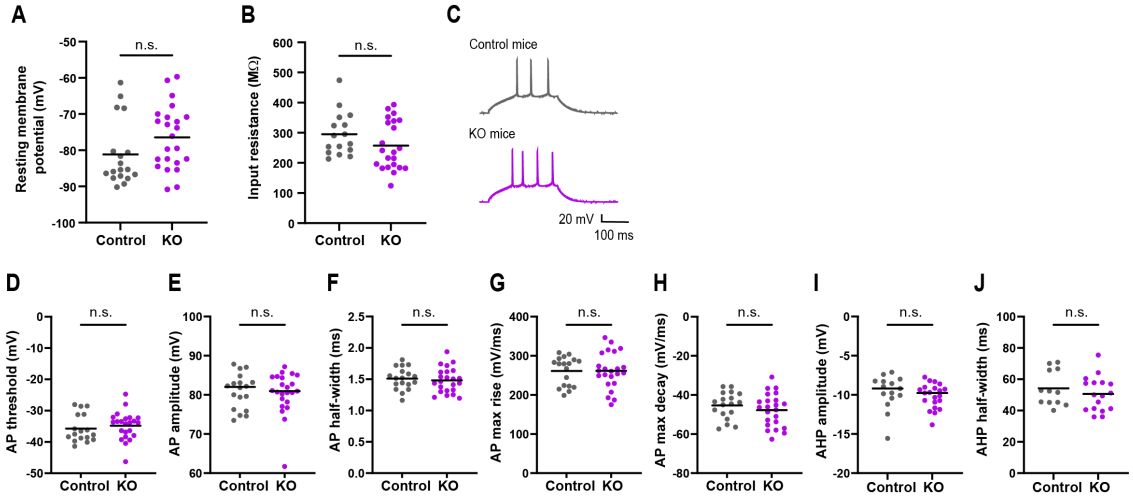

Fig. 3. PV$^+$ neuron-specific *cPcdhγ*KO does not affect the membrane properties of pyramidal neurons.

(A-I) The value of resting membrane potential (A), input resistance (B), AP threshold (D), AP amplitude (E), AP half-width (F), AP max rise (G), AP max decay (H), afterhyperpolarization (AHP) amplitude (I), AHP half-width (J). A bar indicates the median. Mann–Whitney U test, p>0.9999 (E), p=0.2385 (J). A bar indicates the mean. Welch's t test, p=0.1000 (A), p=0.1368 (B), p=0.5076 (D), p=0.6424 (F), p=0.9894 (G), p=0.3180 (H), p=0.4064 (J). control, n=3 mice: KO, n=4 mice. n.s., not significant.

cPcdhγ in PV$^+$ neurons does not affect the pattern and strength of synaptic connections between excitatory and PV$^+$ neurons. Previous studies have shown that cPcdh is involved in the specific reciprocal connection between two excitatory neurons (Tarusawa et al., 2016). To reveal whether cPcdhγ related to the connection specificity between PV$^+$ neuron and Pyr neuron, I conducted simultaneous whole-cell recording in these neuron pairs with cell-to-cell distances within 50 μm (Fig4 A, B). And, to remove samples with poor recording conditions, I exclude the recordings that series resistance (Rs) less than 25 mΩ from analysis (Fig4 C). In control mice, most of the pairs that PV$^+$ and Pyr neurons had inhibitory connections. Approximately 70% of these pairs were in reciprocally connected relationships, forming excitatory synaptic connections from Pyr neurons to PV$^+$ neurons. Excitatory one-way connected pairs were Only 2% (Fig 4D, E). This result is consistent with previous studies showing (Hofer et al., 2011; Znamenskiy et al., 2018). Next, to test for abnormalities in the strength of synaptic connections, I analyzed the synaptic response amplitude between the two neurons. In control mice, the response of unitary inhibitory postsynaptic currents (uIPSCs) was significantly greater in reciprocal pairs than in inhibitory one-way pairs. This is the same result as in the previous study ((Yoshimura & Callaway, 2005). In KO, the same trend as in control uIPSCs, and there was no significant difference from control (Fig 4F). The amplitudes of unitary excitatory postsynaptic currents (uEPSCs) in the reciprocal pairs were also not significantly different between control and KO mice (Fig 4G). These results indicate that

cPcdhγ in PV^+ neurons is not involved in the two-cell connection relationship with Pyr neurons or their synaptic strength.

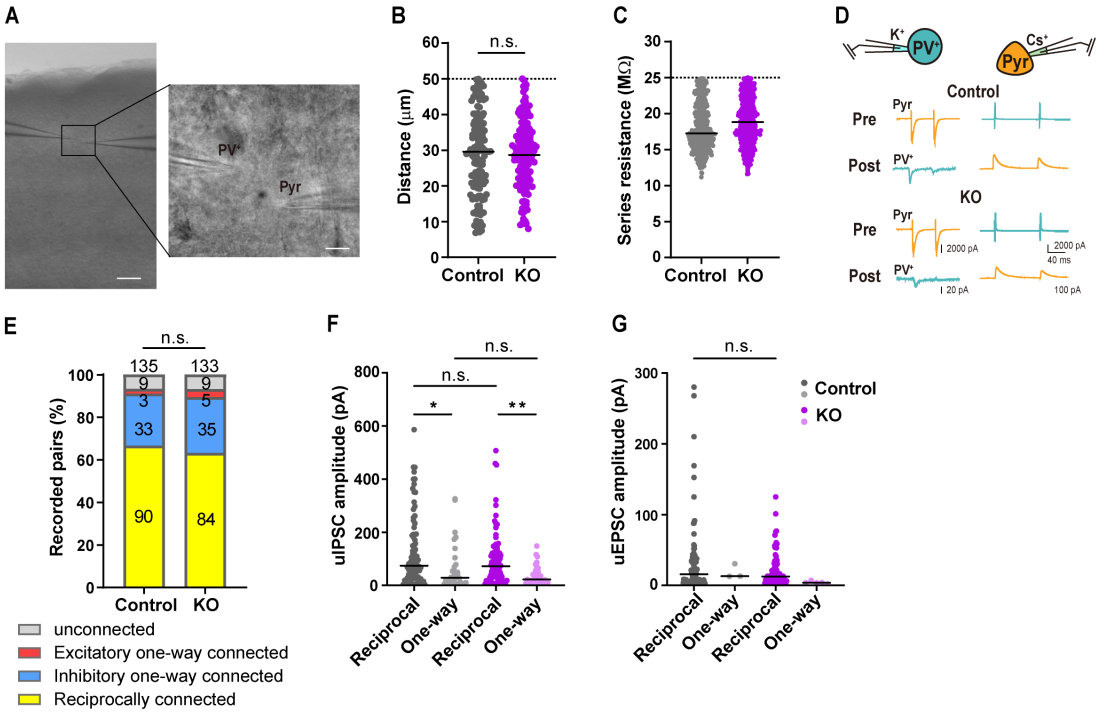

Fig. 4. Connection relationship between PV^+ neuron - Pyr neuron in layer 2/3 of mouse V1.

(A) Differential interference contrast image of a brain slice with recording electrode in a layer 2/3 V1(left). Scale bars, 100 μm. High magnification images of double whole-cell recordings (right). Scale bars, 10 μm. (B) Plot of the distance between PV^+ neuron - Pyr neuron pairs in the control and KO mice. Median is shown. Mann–Whitney U test. P=0.7412. (C) Plot of series resistance of recorded neurons. Median is shown. Notice that there are no neurons more than 25 MΩ. (D) Schematic of double whole-cell recordings form PV^+ neuron - Pyr neuron. K^+-base solution is used for the recording electrode of PV^+ neuron, and Cs^+-base solution is used for the recording electrode of Pyr neuron (top). Representative PV^+ neuron (cyan trace) - Pyr neuron (orange trace) reciprocal pairs average (n=50) traces of presynaptic spikes (pre) by depolarizing voltage pulses and resultant excitatory or inhibitory postsynaptic currents (post) in control mice (middle) and KO mice (bottom). Calibrations are common to all traces. (E) The probability of each connection pattern between PV^+ neuron and Pyr neuron in Control (left) and KO (right) is shown. There was no significant difference between the two groups. Chi-square test, p=0.8612. (F) A plot of uIPSCs amplitude at reciprocally connected (reciprocal, deep color) and inhibitory one-way connected (one-way, light color) from PV^+ neuron to Pyr neuron in control (gray) and KO (purple) mice. One-way ANOVA Kruskal-Wallis test. P=0.0163 (control reciprocal versus control one-way), P=0.0038 (KO reciprocal versus KO one-way), P>0.9999 (control reciprocal versus KO reciprocal), P>0.9999 (control one-way versus KO one-way), P=0.0004 (control reciprocal versus KO one-way), P=0.089 (control one-way versus KO reciprocal). (G) Same as E. But F is a plot of uEPSCs amplitude from Pyr neuron to PV^+ neuron. One-way ANOVA Kruskal-Wallis test. P>0.9999 (control reciprocal versus control one-way), P=0.1352 (KO reciprocal versus KO one-way), P>0.9999 (control reciprocal versus KO reciprocal), P=0.4003 (control one-way versus KO one-way), P=0.0803 (control reciprocal versus KO one-way), P>0.9999 (control one-way versus KO reciprocal). Median are shown; significance is indicated in the figures as follows: *: $P < 0.05$; **: $P < 0.01$; n.s., not significant.

To confirm the anomaly in units of channel expression, I analyzed the waveform kinetics of uIPSCs. In both control and KO mice, six properties that failure event rate of uIPSCs, paired pulse ratio, amplitude, half-width, rise time and decay time were measured and analyzed. There were no significant differences in all measured parameters (Fig 5). This suggests that cPcdhγ in PV^+ neurons could not affect the properties of the channel at inhibitory synapses.

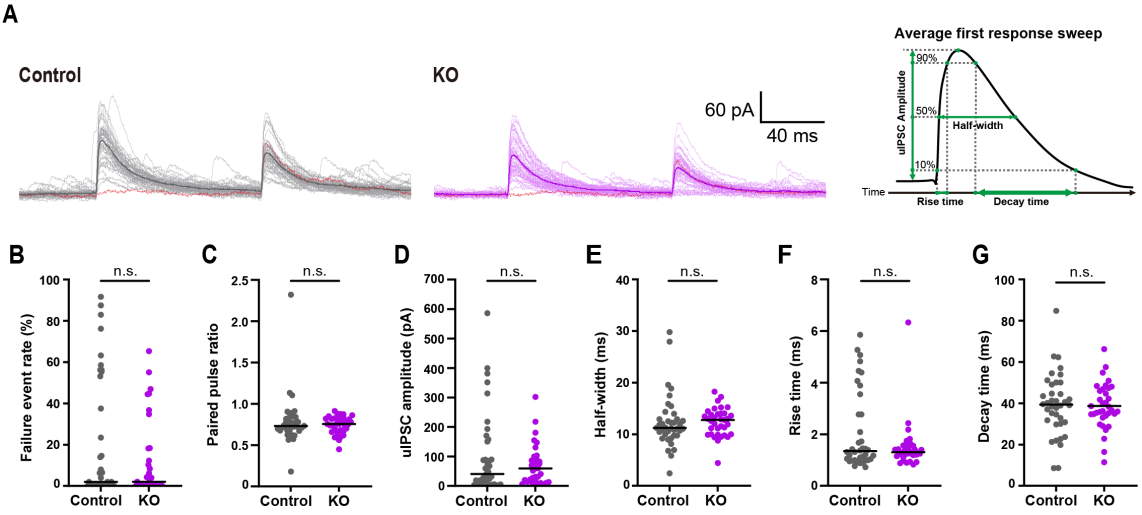

Fig. 5. Waveform kinetics of uIPSCs is normal in PV^+ neuron-specific cPcdhγ KO.

(A) Representative example of a waveform trace (left). Shown are all responses of Pyr neurons to 2 shots of stimulation, 50 times in PV^+ neuron (light color). Red trace indicates miss sweep that no response to the first stimulus (red). The average value of the response excluding miss sweep is shown in dark color. Schematic representation of average uIPSC sweep and each parameter measurement (right). (B) The results of failure event rate are plotted. (C-G) The average uIPSC amplitude excluding miss sweeps is analyzed. (C) The plot shows the paired pulse ratio that response of the second stimulus divided by response of the first stimulus. The value of uIPSC amplitude (D), half-width (E), rise time (F), decay time (G). A bar indicates the median. Mann–Whitney U test, p=0.4744 (B), p=0.7632 (C), p=0.8045 (D), p=0.2352 (E), p=0.7267 (F). A bar indicates the mean. Welch's t test, p=0.8144 (G). n.s., not significant.

cPcdhγ on the postsynaptic side of the PV^+ neuron determines the specificity of local neural circuits.

There was no effect of PV^+ neurons specific cPcdhγ deletion on the connectivity specificity between PV^+ neuron and Pyr neuron. Previous studies have shown specific neural circuits with PV^+ neurons and multiple Pyr neurons in the rat visual cortex layer 2/3 (Yoshimura & Callaway, 2005). Therefore, I tested whether cPcdhγ is involved in that circuit specificity. So, I examined the connection between PV^+ neurons and the two Pyr neurons by simultaneous three whole-cell recordings (fig 6A). I analyzed whether the microcircuitry found in previous studies, in which reciprocally connected PV^+ and Pyr neuron pairs are more likely to receive common input from excitatory cells in layer 2/3 (Yoshimura & Callaway, 2005), and it is disruptive in KO mice. In both control and KO mice, there was no significant difference in common input probability due to

differences in the connection pattern, which has been observed in previous studies (fig 6B). Interestingly, however, PV^+ neurons that reciprocally connected pairs with Pyr neurons had a significantly higher input probability from the other Pyr neurons than that inhibitory one-way connected in control mice. In KO mice, the bias of the input due to such differences in connection pattern was lost (fig 6C). Moreover, results of connection probability in PV^+ - Pyr neuron pairs (Fig 4E) show that when Pyr neurons are excitatory inputs to PV^+ neurons, there is approximately 99 % probability that they are in reciprocal connection in which PV^+ neurons are sending inhibitory inputs to Pyr neurons.

These results suggest that there are two types of PV^+ neurons: the cells tend to make reciprocal connections and the cells do not. To test this hypothesis, I calculated and analyzed the rate at which a PV^+ neuron has reciprocal relationship with neighboring Pyr neurons (Reciprocity of PV^+ neurons value: RPV). The RPV is the number of Pyr neurons with inhibitory synaptic connections divided by the number of Pyr neurons with reciprocal excitatory synaptic connections for a single PV^+ neuron. I was concerned that recording only two Pyr neurons for one PV^+ neuron would bias the RPV to 1/2, so only those that could record connectivity relationships with three or more Pyr neurons were used in the analysis (fig 6D). In control mice, there was a tendency to divide PV^+ neurons with high rate of reciprocal connected (High-RPV, 75%) and with low rate (Low-RPV, approximately 17%). In KO mice, there was a decrease in the percentage of PV^+ neurons with High-RPV (approximately 36%) and an increase of PV^+ neurons with RPV less than 1.0 and greater than 0.5 (Mid-RPV, approximately 64%) (fig 6E). This result supports the hypothesis that PV^+ neurons can be classified into different types according to their connection pattern. Moreover, show similar trend to the results of the probability of excitatory input to PV^+ neurons and that specificity is collapsed in PV^+ neurons specific cPcdhγ deletion (fig 6C).

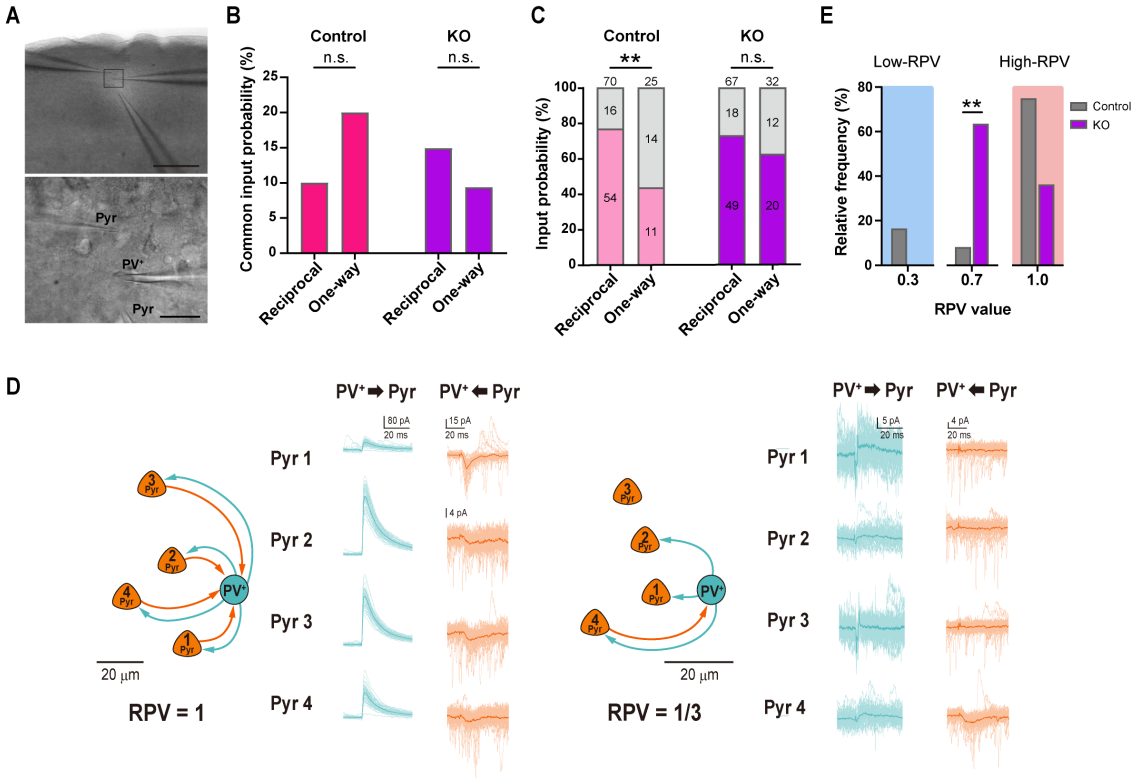

Fig. 6. cPcdhγ of PV$^+$ neurons is involved in determining the specificity of local neural circuits centered on PV$^+$ neurons.

(A) Differential interference contrast image of a brain slice with recording electrode in a layer 2/3 V1(left). Scale bars, 200 μm. High magnification images of triple whole-cell recordings (right). Scale bars, 20 μm. (B) The probability of common input that PV$^+$- Pyr neuron pairs received from the other Pyr neurons are shown in reciprocal (left) and inhibitory one-way connections (right) of control (pink) and KO mice (purple), respectively. Fisher's exact test. P=0.2901 (control reciprocal versus control one-way), P=0.5391 (KO reciprocal versus KO one-way), P=0.4433 (control reciprocal versus KO reciprocal), P=0.2799 (control one-way versus KO one-way). control, n=95 pairs (reciprocal: 70 pairs, one-way: 25 pairs): KO, n=99 pairs (reciprocal: 67 pairs, one-way: 32 pairs). (C) Same as B. But C is a plot of the probability of received excitatory input from the other Pyr neurons in PV$^+$ neurons. Fisher's exact test. P=0.0049 (control reciprocal versus control one-way), P=0.3508 (KO reciprocal versus KO one-way), P=0.6931 (control reciprocal versus KO reciprocal), P=0.1899 (control one-way versus KO one-way). (D) Representative example of the actual connection relationship between recording neurons centered on PV$^+$ neuron and those wave traces. Shown are all response traces of Pyr neurons (cyan) and PV$^+$ neuron (orange) except trace that with a misaligned baseline and that is blind to the response in spontaneous activity (light color). The average trace excluding miss sweep is shown in dark color. The left group centered on PV$^+$ neuron was in reciprocal connected relationship with all recorded Pyr neurons. While, the right group centered on PV$^+$ neuron was inhibitory connected to three Pyr neurons, one of which are responsible for excitatory input to the PV$^+$ neurons. (E) The distribution of RPV was represented by a histogram (0.3 bin: RPV value 0.26 – 0.34, 0.7 bin: RPV value 0.66 – 0.74, 1.0 bin: RPV value 1.0). Fisher's exact test. P=0.4783 (0.3 bin), P=0.0094 (0.7 bin), P=0.0995 (1.0 bin). control, n=12 groups: KO, n=11 groups. Significance is indicated in the figures as follows: **: P < 0.05; n.s., not significant.

These results indicate that PV^+ neurons have specific local neural circuits with different connectivity between multiple neighboring Pyr neurons in layer 2/3 of V1, which is lost by PV^+ neurons specific cPcdhγ KO. In order to confirm the difference between these two types of local neural circuits in detail, I measured and analyzed the kinetics of uIPSC and uEPSC at each RPV group (Fig 7). Among the eight measurements parameter, there was a significant difference between Low and High-RPV groups for uIPSC amplitude, failure event rate and paired pulse ratio in control mice (Fig 7A, E, F). However, there was no significant difference between such RPV groups in KO mice. These results indicate that these two types of local neural circuits are not only different in their connectivity centered on PV^+ neurons, but also in the intensity of their inhibitory input.

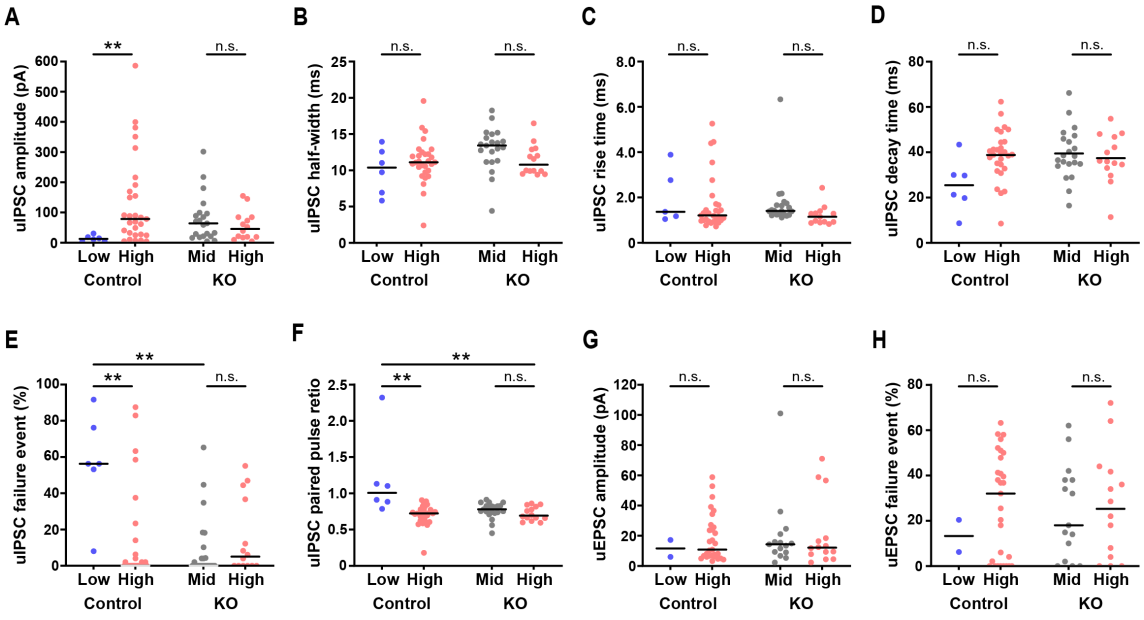

Fig. 7. Groups of RPVs also differ in some parameters of uIPSCs.

(A) Plot of the uIPSC amplitude in each RPV groups. One-way ANOVA Kruskal-Wallis test. Median are shown; P=0.0081 (control Low-RPV versus control High-RPV), P>0.9999 (KO Middle-RPV versus KO High-RPV), P=0.0534 (control Low-RPV versus KO Middle-RPV), P=0.7573 (control High-RPV versus KO High-RPV), P=0.3251 (control Low-RPV versus KO High-RPV), P>0.9999 (control High-RPV versus KO Middle-RPV). (B) Same as A. But B is a plot of uIPSC half-width. One-way ANOVA Kruskal-Wallis test. Median are shown; P>0.9999 (control Low-RPV versus control High-RPV), P=0.2241 (KO Middle-RPV versus KO High-RPV), P=0.1358 (control Low-RPV versus KO Middle-RPV), P>0.9999 (control High-RPV versus KO High-RPV), P>0.9999 (control Low-RPV versus KO High-RPV), P=0.0608 (control High-RPV versus KO Middle-RPV). (C) Same as A. But C is a plot of uIPSC rise time. One-way ANOVA Kruskal-Wallis test. Median are shown; P>0.9999 (control Low-RPV versus control High-RPV), P=0.069 (KO Middle-RPV versus KO High-RPV), P>0.9999 (control Low-RPV versus KO Middle-RPV), P>0.9999 (control High-RPV versus KO High-RPV), P=0.727 (control Low-RPV versus KO High-RPV), P=0.4668 (control High-RPV versus KO Middle-RPV). (D) Same as A. But D is a plot of uIPSC decay time. One-way ANOVA One-way ANOVA Dunnett's T3 multiple comparisons test. Mean are shown; P=0.1759 (control Low-RPV versus control High-RPV),

P=0.9943 (KO Middle-RPV versus KO High-RPV), P=0.1522 (control Low-RPV versus KO Middle-RPV), P=0.999 (control High-RPV versus KO High-RPV), P=0.2809 (control Low-RPV versus KO High-RPV), P>0.9999 (control High-RPV versus KO Middle-RPV). (E) Same as A. But D is a plot of uIPSC failure event rate. One-way ANOVA Kruskal-Wallis test. Median are shown; P=0.0032 (control Low-RPV versus control High-RPV), P>0.9999 (KO Middle-RPV versus KO High-RPV), P=0.007 (control Low-RPV versus KO Middle-RPV), P>0.9999 (control High-RPV versus KO High-RPV), P=0.0546 (control Low-RPV versus KO High-RPV), P>0.9999 (control High-RPV versus KO Middle-RPV). (F) Same as A. But F is a plot of uIPSC paired pulse ratio. One-way ANOVA Kruskal-Wallis test. Median are shown; P=0.0011 (control Low-RPV versus control High-RPV), P=0.7373 (KO Middle-RPV versus KO High-RPV), P=0.0801 (control Low-RPV versus KO Middle-RPV), P>0.9999 (control High-RPV versus KO High-RPV), P=0.0035 (control Low-RPV versus KO High-RPV), P=3675 (control High-RPV versus KO Middle-RPV). (G) Same as A. But G is a plot of uEPSC amplitude. One-way ANOVA Kruskal-Wallis test. Median are shown; P>0.9999 (control Low-RPV versus control High-RPV), P>0.9999 (KO Middle-RPV versus KO High-RPV), P>0.9999 (control Low-RPV versus KO Middle-RPV), P>0.9999 (control High-RPV versus KO High-RPV), P>0.9999 (control Low-RPV versus KO High-RPV), P>0.9999 (control High-RPV versus KO Middle-RPV). (H) Same as A. But H is a plot of uEPSC failure events rate. One-way ANOVA Kruskal-Wallis test. Median are shown; P>0.9999 (control Low-RPV versus control High-RPV), P>0.9999 (KO Middle-RPV versus KO High-RPV), P>0.9999 (control Low-RPV versus KO Middle-RPV), P>0.9999 (control High-RPV versus KO High-RPV), P>0.9999 (control Low-RPV versus KO High-RPV), P>0.9999 (control High-RPV versus KO Middle-RPV). Significance is indicated in the figures as follows: **: $P < 0.05$; n.s., not significant.

cPcdhγ in PV$^+$ neuron is involved in the determination of layer-specific excitatory inputs.

I revealed new local neural circuits of PV$^+$ neurons with neighboring excitatory neurons, and its specificity was related to cPcdhγ in PV$^+$ neurons. cPcdhγ of PV$^+$ neuron in layer 2/3 can affect not only local circuits with neighboring Pyr neurons, but also input specificity between excitatory neurons in other layers. So, to clarify the function of cPcdhγ in PV$^+$ neurons in other layers of the V1, I conducted laser scanning photostimulation (Yoshimura & Callaway, 2005). In this experiment, I used Ruthenium-bipyridine-trimethyl phosphine-Glutamate (Rubi-Glutamate). The cage has the property of releasing glutamate by photo-cleavage within nanoseconds when absorbing one photon of visible light or two photons of near-infrared light. Recording within this reagent enables selective firing of neurons in any spot on the slice (Fig 8A). The mean amplitude of the excitatory input received by the PV$^+$ neuron of layer 2/3 from layer 2 - 6 tended to be larger in KO mice than in control and was significant for the mean input frequency. Comparing the results for each layer individually, KO mice showed a significant increase in the amplitude and frequency of excitatory input from layers 5 and 6 (Fig 8B, C).

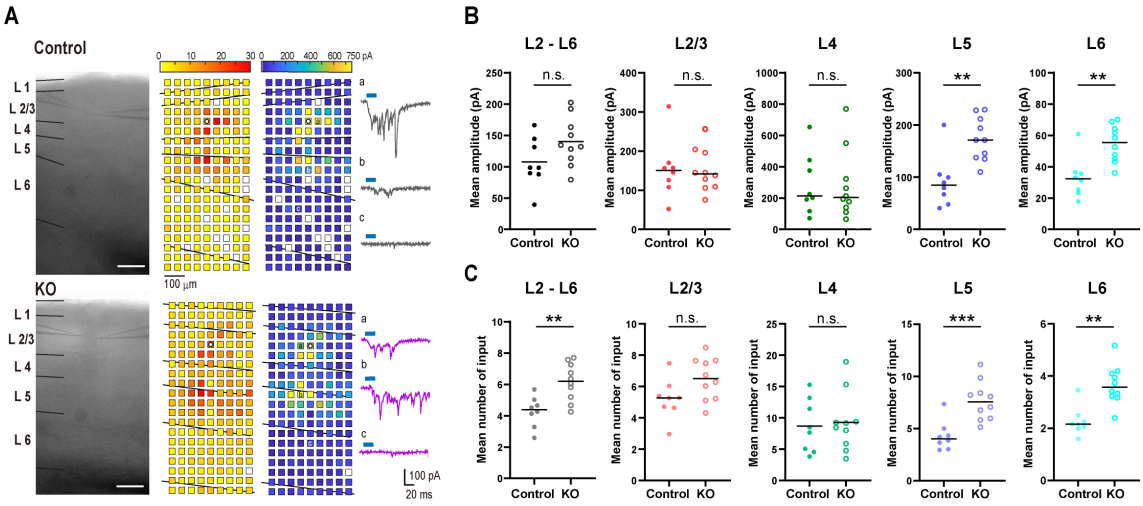

Fig. 8. PV$^+$ neuron-specific deletion of cPcdhγ increases the excitatory input that layer 2/3 PV$^+$ neurons receive from layer 5 and 6.

(A) Differential interference contrast image of a brain slice with recording electrode in a layer 2/3 V1(left). Scale bars, 200 µm. The frequency (middle left) and amplitude (middle right) of the recorded PV$^+$ neuron (white circle) response is shown as a color map within a square at each location where the photostimulus was exposed. The response traces of the actual PV$^+$ neurons to photostimulation at each spot are presented on the right. The blue bar shows the laser exposure time. (B) The mean amplitude of photostimulus excitatory response for each layer was plotted. A bar indicates the median. Mann–Whitney U test, p=0.8286 (L2/3), p=0.8286 (L4), p=0.0021 (L5), p= 0.0021(L6). A bar indicates the mean. Welch's t test, p=0.0967 (L2-6). (C) Same as B. But C is the mean frequency of the photostimulus excitatory response. A bar indicates the median. Mann–Whitney U test, p=0.0009 (L5), p= 0.0014(L6). A bar indicates the mean. Welch's t test, p=0.0019 (L2-L6) p=0.0574 (L2/3), p=0.7876 (L4). Significance is indicated in the figures as follows: **: P < 0.005; ***: P < 0.001; n.s., not significant. control, n=8 neurons: KO, n=10 neurons.

From the results of Chapter 1 (Fig 6,7), it is clear that there are two types of PV$^+$ neurons with different local circuits. I confirmed that the rate of input from each layer was different for each PV$^+$ neuron (Fig 9A). In control, there were many PV$^+$ neurons with the highest rate of input from layer 2/3, and among them, two types were found (Proportion of 5/8). One type was seen with less input from layer 4, more from layer 5, and as little as layer 4 from layer 6 (“h” shape type). Another type was seen from L2/3 to the lower layers, with less and less input (downward type). Some cells had the highest rate of input from layer 4 (layer 4 peak type). These cells had the next highest rate of input from layer 2, and layers 5 and 6 tended to be equally low. On the other hand, in KO mice the rate of input from layer 2/3 was lower than control, but a group of cells that resembled the “h” shape and layer 4 peak type was found (Proportion of 1/2 and 3/10). However, a new type of PV$^+$ neurons were found in the KO that was not found in the control. It was receiving the most excitatory input from layer 5 (Fig 9B).

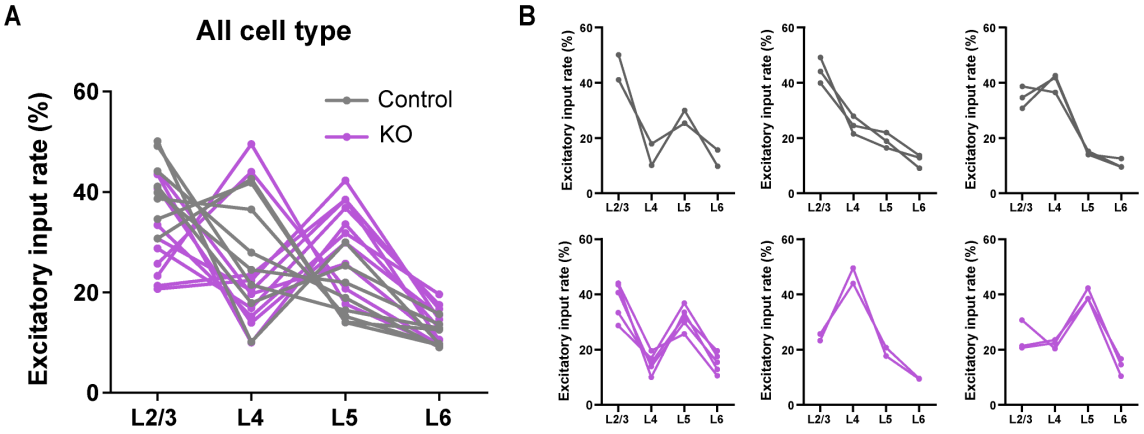

Fig. 9. Characterization of PV$^+$ neurons by the rate of excitatory input from each layer.

(A) The line graphs show the layer-specific input rates of all PV$^+$ neurons for control (gray) and KO (purple), respectively. (B) The control and KO mice of the data in A are shown separately for each input rate type.

These suggest that there are several specificity types of input rates from each layer to the PV$^+$ neurons and, more interestingly, that cPcdhγ in the PV$^+$ neurons could be involved in determining its specificity.

Chapter 2
Relationship between PV+- Pyr neuron connectivity and expression of each isoform of cPcdh.

Expression specificity of cPcdh in PV+ and Pyr neurons.

In Chapter 1, I found that two types of PV+ neurons are observed in layer 2/3 of the V1 and that they form distinct connectivity relationships with neighboring Pyr neurons. They also found that PV+ neuron-specific deletion of cPcdh resulted in abnormal binding relationships with multiple Pyr neurons. Furthermore, I found that PV+ neurons specific deletion of cPcdhγ resulted in irregularities in the connection with multiple Pyr neurons (Fig 6,7). Previous studies have shown that cPcdhγ inhibits synaptogenesis at the postsynapse by interacting with Neuroligin-1, which is a synaptogenesis factor. Moreover, it has been reported that cPcdh isoforms expressed on the cell membrane have homophilic interactions with isoforms of the same type that exist on the membranes of different cells. Moreover, cPcdhγ has been shown to be removed from the membrane by matrix metalloproteinases and other mechanisms in *vitro* studies (Haas et al., 2005, Reiss et al., 2006). Based on these findings, it has been hypothesized that when cPcdhγ isoforms are matched pre and postsynapses, the interaction between Neuroligin-1 and cPcdhγ is lost, resulting in the formation of a specific synapse (Molumby, M.J. et al., 2017). Therefore, I proposed the following hypothesis about the role of cPcdhγ in the formation of these two specific circuits (Fig 10). Low-RPV has a low number of excitatory synaptic connections because the low number of cPcdhγ isoforms expressed at the postsynapse reduces the number of matches in relation to the cPcdhγ isoforms existing at the presynapse, and thus synaptogenesis by Neuroligin-1 remains inhibited. Conversely, High-RPV has a higher number of cPcdhγ isoforms expressed at the postsynapse, which increases the relative number of matches with cPcdhγ isoforms at the presynapse, resulting in the release of synaptic inhibition and a higher number of excitatory synaptic connections.

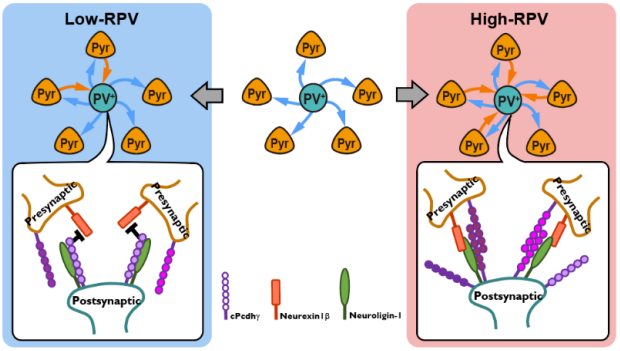

Fig. 10. Role of cPcdhγ in the formation of specific local circuits around PV+ neurons.
The hypothesis of a mechanism involving cPcdhγ in the formation of High and Low-RPV.

To confirm the hypothesis that the number of cPcdhγ isoforms expressed is involved in the

formation of two specific local circuits, I performed single-cell RamDA patch sequencing after simultaneous cell recording of PV^+ and Pyr neurons (Fig 11). First, I examined whether there is a specificity of expression of cPcdh isoforms for each cell type in layers 2/3 of the mouse V1. For the variable isoform of cPcdh, there was almost no significant difference between the two cell types. However, it is interesting to note that the constitutive (C-type) isoform, cPcdhγC4, tend to be highly expressed in PV^+ neurons rather than in Pyr neurons, while cPcdhγC5 is significantly more expressed in Pyr neurons (Fig 11 B-E). Next, I analyzed whether there was also cell-type specificity in the number of isoforms expressed. There was no significant difference between the two cells for all cPcdh isoforms expressed in the cells and for the variable isoforms, but the C-type isoforms were significantly more expressed in PV^+ neurons (Fig 11F). This is thought to be caused by the low expression rate of γC4 in Pyr neurons. The expression specificity of the variable isoforms in each cluster showed that the total number of cPcdhγ isoforms was significantly lower in PV^+ neurons than in Pyr neurons (Fig 11G). Next, to clarify the hypothesis discussed in figure 10 I confirmed the number of cPcdh isoforms expressed in PV^+ neurons. The distribution of the number of cPcdh isoforms per cell in Pyr neurons was almost evenly distributed in both the only variable isoform and total γ cluster isoforms. As expected, the expression of PV^+ neurons and total γ clusters was not uniformly distributed and tended to vary between cells with high and low numbers of expressed isoforms. In addition, PV^+ neurons with more isoform expression tended to be present in greater numbers than those with less (Fig 11H). This shows a similar trend to the High and Low-RPV distributions. Interestingly, the expression of only variable isoforms showed an evenly distributed variability. This suggests that the C-type isoform of cPCdhγ is involved in determining the specificity of local neural circuits.

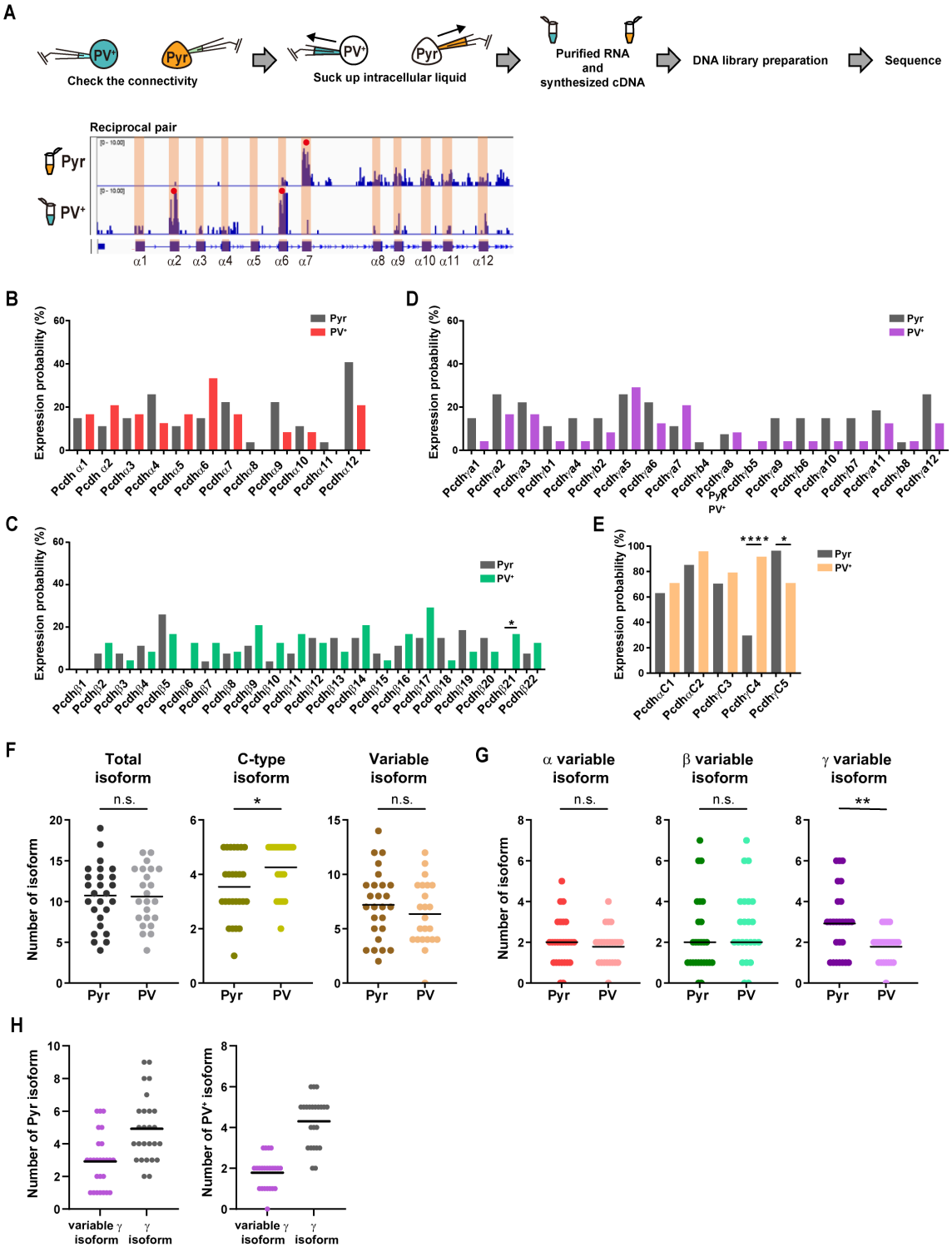

Fig. 11. Expression characteristics of cPcdh isoforms in PV$^+$ and Pyr neurons

(A) Schematic diagram of the single-cell RamDA patch sequencing procedure (top). First, I will do a double whole-cell patch of PV$^+$ - Pyr neurons to check the relationship. Then, by applying negative pressure to the glass electrode, intracellular fluid is sucked out, and cDNA is synthesized and sequenced

from the sample. Sequencing results of samples taken from bidirectional pairs, with reading maps for each isoform of cPcdhα represented as histograms (bottom). From this result, the expression was binarized according to the criterion. (B-E) Represents the expression probability of each cPcdh isoform. cPcdhα variable isoform (B), cPcdhβ variable isoform (C), cPcdhγ variable isoform (D), cPcdh constitutive isoform (E). Fisher's exact test. P=0.0418 (Pyr-b21 versus PV-b21), P<0.0001 (Pyr-gC4 versus PV-gC4), P=0.0072 (Pyr-gC5 versus PV-gC5). (F) The plot of the total number of isoform expressions of cPcdh isoform (left), C-type isoform (middle), and variable isoform (right). A bar indicates the mean. Welch's t-test, p=0.9075 (left), p=0.0223 (middle), p=0.3371 (right). (G) Same as E. But G is the plot of the number of expressed isoforms for each cluster within a variable isoform. Welch's t-test, p=0.4743 (cPcdhα), p=0.0033 (cPcdhγ). A bar indicates the median. Mann–Whitney U test, p=1911 (cPcdhβ). (H) The plot of the number of cPcdhγ only variable and γ cluster total isoforms expressed in Pyr (left) and PV^+ neuron (right), respectively. Pyr, n=27 neurons: PV^+, n=24 neurons. Significance is indicated in the figures as follows: *: P < 0.05; **: P < 0.01; ****: P < 0.0001; n.s., not significant.

Relationship between the match of expression cPcdh isoforms and connection specificity in PV^+ - Pyr neurons.

Because cPcdh has a homophilic intercellular interaction, it has been remarked that there is a relationship between the number of cPcdh isoform matches and synapse formation. Actually, excitatory sister cells in layer 4 in the somatosensory cortex, which are differentiated from the same stem cells, tend to connect with each other and also have a higher number of cPcdh isoform matches, as reported in this laboratory (Masuda, in preparation). Therefore, it is possible that excitatory and inhibitory neurons in a connective relationship also express the same type of cPcdh isoform. To clarify this, I analyzed the number of matched isoforms in PV^+-Pyr reciprocal pairs. Compared to the shuffle group, the reciprocal pair had a higher probability of matching the total cPcdh isoforms. Surprisingly, the expression match rate of only variable isoforms was not different from the shuffle group, while the match rate of only C-type was significantly higher than the shuffle group (Fig 12A). The expression match rate of variable isoforms in each cluster also did not differ from the shuffle group (Fig 12B). Next, I analyzed which isoforms are more likely to be matched in PV^+-Pyr reciprocal pairs. There was not significantly higher than the shuffle group (Fig 12C-F).

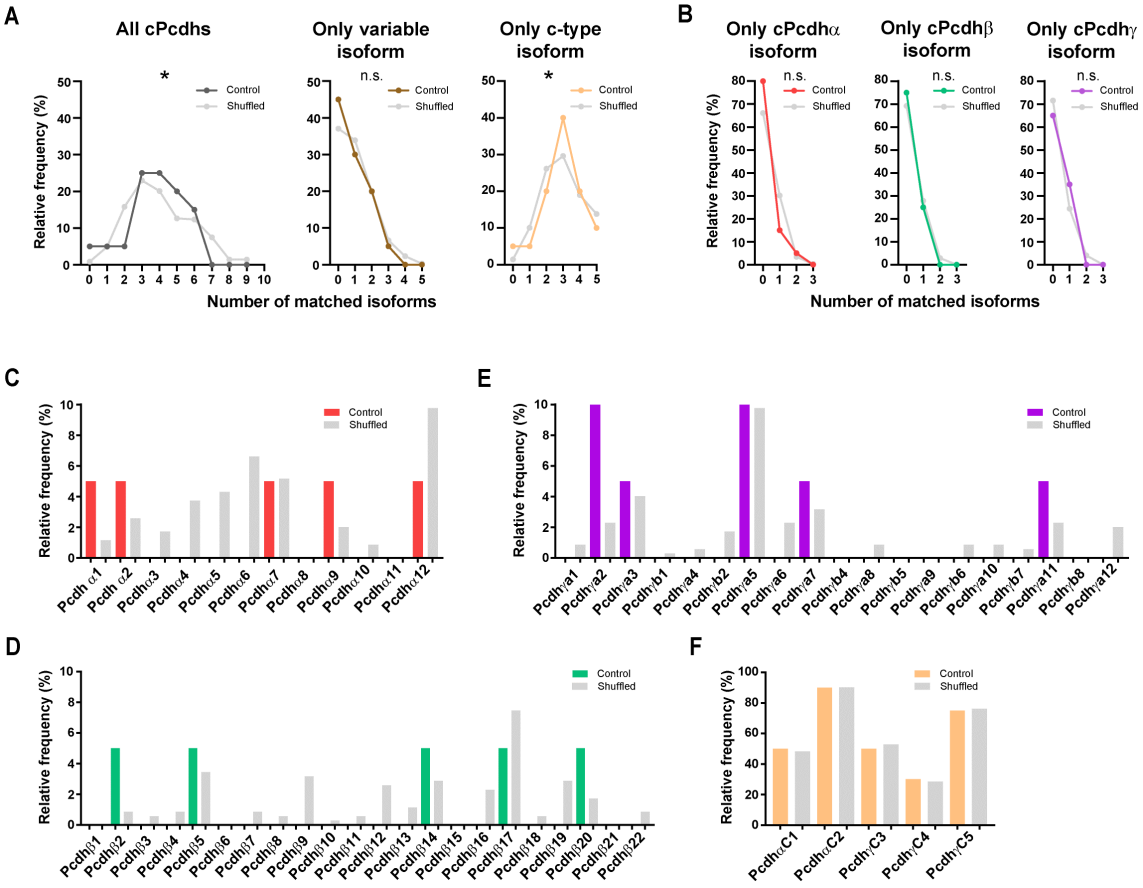

Fig. 12. Match rate of expressed isoforms in PV^{+}-Pyr reciprocal pairs.

(A) The plot of isoform match rates for all cPcdh (left), only variable (middle), and only C-type isoforms (left). Kolmogorov–Smirnov test, P=0.0101 (left, control versus shuffle), P=0.1429 (middle, control versus shuffle), P=0.026 (left, control versus shuffle). (B) Same as A, but B is the plot of the number of variable isoforms matches in each cluster. Kolmogorov–Smirnov test, P=0.6571 (left, control versus shuffle), P=0.6571 (middle, control versus shuffle), P=0.2286 (left, control versus shuffle). (C-F) Histogram of the probability of each isoform match between PV^{+}-Pyr reciprocal pairs. control; n=20 pairs. Fisher's exact test. All nonsignificant. Significance is indicated in the figures as follows: *: P < 0.05; n.s., not significant.

Discussion

In this study, to clarify the local neural circuit between excitatory Pyr neurons and PV^+ inhibitory neurons in mice and to investigate the role of cPcdhγ in PV^+ neurons in the local neural circuit, I conducted an electrophysiological analysis of the connection specificity between multiple cells using control and $cPcdh\gamma^{PV\text{-}Cre}$ mice. The pattern and strength of connectivity between the two cells were not significantly affected by the deletion of cPcdhγ. On the other hand, I found new local circuits, one with more and another with less reciprocal connections with multiple neighboring Pyr neurons, centered on PV^+ neurons. Surprisingly, the results revealed that the specificity of this local neural circuit is lost by PV^+ neuron-specific cPcdhγ deletion. In this study, I also found that PV^+ neurons in L2/3 received different rates of excitatory input in different layers. Furthermore, the cPcdhγ of PV^+ neurons were shown to be involved in the input rate of its layer-specific excitability (Fig 13).

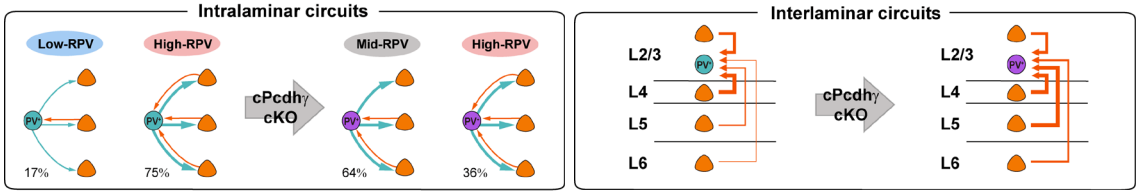

Fig. 13. Local neural circuits between PV^+ neurons and excitatory neurons and the effect of PV^+ neuron-specific cPcdhγ KO in the primary visual cortex of mice.

Model diagram showing the local neural circuitry and the effects of cPcdhγ KO among excitatory neurons, centering around PV^+ neurons in the intralaminar (left) and interlaminar (right) that found in this study.

The relationship between PV^+ neurons and Pyr neurons in the L2/3 layer of the primary visual cortex.

In the probability of connectivity between PV^+ and Pyr neurons, the pair with inhibitory connectivity was about 91% of the total in this experiment. This result is consistent with previous studies (88% of the total) (Hofer et al., 2011). The amplitude of uIPSCs in those pairs was significantly larger when they were reciprocally connected than when they were inhibitory one-way connected. This is consistent with previous studies in rats (Yoshimura & Callaway, 2005), indicating that the same characteristics are present in mice. In contrast, in the previous study, I was unable to confirm a microcircuit (Yoshimura & Callaway, 2005) in which pairs received a predominantly higher probability of common inputs from other excitatory cells when they are reciprocal connection than when inhibitory one-way connection. There are two reasons for this. One is that the method in this study is different from that used in previous studies. In a previous study, it was analyzed using photostimulated uncaging with caged glutamate in the extracellular fluid. After simultaneously recording pairs, randomly exposing the cells to laser at one spot will

cause them to fire, and cross-correlation is used to analyze whether the pair is receiving a common input. The disadvantages of this method are the possibility of firing multiple cells due to the laser spot, and the possibility of incorrect cross-correlation due to the spontaneous activity of the cells. On the other hand, the method of this study uses patch clamping of three cells at the same time, so it is more reliable than the previous method that the inputs from a single cell. In addition, it is possible to distinguish between spontaneous activity and response because responses to two stimuli are observed. Another reason could be the difference in circuit specificity between animal species. The differences between mice and rats are not clear. In this study, I referred only to the differences in microcircuitry between the three cells but also differed in the connection pattern of PV^+- Pyr neuron pairs (Wonders & Anderson, 2006). These results suggest that the circuitry of the V1 could be different even in the same rodent.

Connection specificity between PV^+- Pyr neuron pairs and the effect of cPcdhγ deletion.

No significant effect of PV^+ neuron-specific deletion of cPcdhγ was observed in the PV^+- Pyr connection relationship between the two cells. Previous analyses in my laboratory have shown that inhibitory neuron-specific deletion of cPcdhγ reduced inhibitory synaptic inputs to excitatory neurons in layer 4 of the somatosensory cortex (Adach, in preparation). In addition, it has become clear that this disorder is caused by the cell death of inhibitory neurons that occurs during the development of the cerebral cortex (Ariga, in preparation). In that study, cPcdhγ is deleted specifically in inhibitory neurons by *Dlx5/6*-Cre. *Dlx5/6* is expressed around 12 days of embryogenesis (Wonders & Anderson, 2006), suggesting that the loss of cPcdhγ in early development is involved in the cell death of inhibitory neurons. In contrast, I was able to test whether cPcdhγ is involved in the formation of neural circuits without being affected by cell death in early development by expressing Cre under the regulation of PV promoter activity, which occurred after 7 days of age in the cerebral cortex. Such a delay in the deletion of cPcdhγ is thought to be the reason for the severe phenotype not observed in mice that previously deletion cPcdhγ in inhibitory neurons. However, in this study, I found that the deletion of cPcdhγ in PV^+ neurons tends to affect the formation of local neural circuits with multiple Pyr neurons.

Two types of local neural circuits with multiple Pyr neurons centered on PV^+ neurons.

In this experiment, I found that there are two types of cells for the first time: PV^+ neurons that have a high probability of reciprocal connections with multiple neighboring Pyr neurons (High-RPV) and a low probability of reciprocal connections (Low-RPV). This result indicates that the local neural circuits are different depending on the type of PV^+ neurons. It is known that PV^+ neurons, a type of inhibitory neuron, can be classified into two types, basket cells and chandelier

cells, according to their morphological characteristics and membrane properties, even though they show the same PV^+ neurons fast-spiking behavior (DeFelipe, 1997; DeFelipe et al., 1999; Kisvárday and Eysel, 1993; Markram et al., 2004). PV^+ neurons in the visual cortex have been analyzed in more detail, and it has been reported that there are several types of basket cells depending on the mRNA expressed and cell morphology (Gouwens et al., 2019). In addition, it has been reported that each basket cell has different visual response characteristics (Hofer et al., 2011) and different dendritic morphology (Runyan et al., 2013). Recently, it has also been reported that there are PV^+ neurons with different rates of reciprocal connections in other brain regions (Peng et al.,2021). This suggests that the specificity observed in the control mice is due to the different reciprocal connections of each PV^+ neuron.

I was unable to clarify the functional meaning of the two types of connection specificity centered on PV^+ neurons that I found in this study. There are two hypotheses about the functional differences between these two types of local neural circuits. One is the involvement of the visual stimulus-response on the preference. It has been shown that excitatory neurons in the primary visual cortex have a high degree of orientation selectivity, which means that they are active only to visual stimuli of a specific orientation. However, most PV^+ neurons have a low orientation selectivity in that they are active in any orientation visual response. However, there are PV^+ neurons with high selectivity at a low rate of approximately 18% (Hofer et al., 2011). This result is similar to the rate of Low-RPV (approximately 17%) in this experiment. Each Pyr neurons have a variety of orientation selectivity. PV^+ neurons, which are reciprocally connected to many Pyr neurons (High-RPV), can respond to many orientations and become less orientation-selective because they are receiving input from the many Pyr neurons. On the other hand, PV^+ neurons that have reciprocal connections with only a few Pyr neurons (Low-RPV) can be estimated to have a biased orientation selectivity. The other difference is due to the input from the thalamus. Excitatory input from the lateral geniculate nucleus (LGN) in the thalamus is mainly projected to layer 4, but there are also patchy projection areas in layer 1. The PV^+-Pyr pairs in layer 2/3 under the patch showed a significantly smaller uIPSC amplitude received by the Pyr neurons and a significantly larger rise time than the pair under the non-patch, although the connection probability did not differ (D'Souz et al., 2019). In this study, I found that PV^+ neurons in the two types of local neural circuits were significantly different not only in the rate of bidirectional connections, but also in the amplitude of uIPSCs. In this study, it is considered that the difference in rise time could not be seen due to the small number of experiments. These suggest that the input from the thalamus and the histological location of its neurons may be different between High and Low-RPV.

Although it was not confirmed in this study, previous studies have also reported that PV^+ neurons with high orientation selectivity have different dendritic morphology compared to with low selectivity. It is highly possible that these two types of PV^+ neurons are different not only in their reciprocal connection probability and uIPSC response properties but also in their cell morphology. In addition, the reciprocal connection probability of PV^+ neurons branch is different across the dendritic morphology and the location of the cell bodies of Pyr neurons in the superficial presubiculum (Peng et al.,2021).

Circuit anomaly due to PV^+ neuron-specific cPcdhγ deletion observed only in three or more cells.

In this study, I found abnormalities due to PV^+ neuron-specific cPcdhγ deletion in local neuronal circuits between multiple Pyr neurons, centered on PV^+ neurons, even though the pattern and probability of PV^+-Pyr connections were the same as in control mice. In order to investigate whether this phenomenon can be observed, I created a simple model diagram based on the observed results of the connection probability between two cells (Fig. 14).

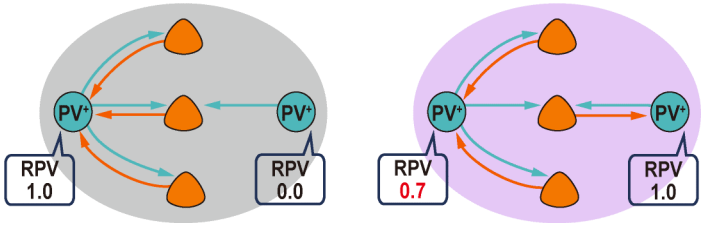

Fig. 14. Connection probability and RPV value

The left and right populations have the same number of excitatory and inhibitory neurons and connection probability between the two cells. However, the RPV values are different between the populations.

In the two populations with the same number of excitatory and inhibitory connections, the left population has high and low RPVs, while in the right population, low RPVs are lost. This is not inconsistent with the findings that PV^+ neuron-specific cPcdhγ deletion does not affect the probability or strength of synaptic connections between two cells, but does affect the specificity of connections with multiple Pyr neurons.

Layer-specific excitatory input to PV^+ neurons in layer 2/3 and abnormalities caused by cPcdhγ deletions.

In this study, I found that the loss of PV^+ neuron-specific cPcdhγ significantly increased the excitatory input received by PV^+ neurons in layer 2/3 from layer 5 and 6. There are two major possible causes for this. One is a disruption of the local neural circuitry centered on the PV^+ neuron in layer 2/3. PV^+ neurons in layer 2/3 also mainly inhibitory connections of excitatory neurons in

L2/3. (McColgan et al., 2020). PV^+ neuron-specific cPcdhγ KO decreases the proportion of High-RPVs compared to control mice, thus decreasing the excitatory input received and the activity of PV^+ neurons. This could increase the excitatory input from layer 5 by decreasing the inhibitory input to the excitatory neurons in layer 2/3. In addition, Low-RPV was not observed in KO mice. PV^+ neurons in layer 2/3 may have inhibitory projections to PV^+ neurons in layer 5. This suggests that inhibitory input from PV^+ neurons in layer 2/3 to PV^+ neurons in other layers increases more than the excitatory input they receive, which could decrease inhibitory input to Pyr neurons in layer 5 and increase excitatory input due to disinhibition. Probably, it is more likely to be the first, based on the ratio of High-RPV and Low-RPV.

Another reason is the disruption of neural circuits within layer 5. It is possible that the local neural circuit abnormality centered on PV^+ neurons, which was revealed in this study, also exists in layer 5. Moreover, I only confirmed the cell-to-cell connection in layer 2/3, so it cannot exclude the possibility that not only the local neural circuitry but also the synaptic connection probability differs in layer 5 for PV^+ neuron-specific cPcdhγ KO. Thus, this could be due to abnormalities caused by layer-specific excitatory neuron types. At this stage, it remains unclear which layers are causing the layer-specific interlaminar neural circuits disorder through local circuit abnormalities.

In control mice, the PV^+ neurons in layer 2/3 received the most excitatory input from the same layer compared to the other layers. There have been no studies that compare the layer-specific excitatory inputs to PV^+ neurons in the L2/3 layer. This study showed that this layer specificity was not constant among PV^+ neurons, and three types of layer specificity were confirmed. In KO mice, most of the cells tended to be like controls, but some PV^+ neurons with completely different layer specificity were also observed. This phenomenon of abnormalities in only some neuron types is similar to the disorder of local neural circuits observed in layer 2/3. This suggested that the role of cPcdhγ in PV^+ neurons is not constant and could vary depending on the neuron type.

Role of cPcdhγ on the specificity of two types of local neural circuits in layer 2/3.

I hypothesized that the involvement of cPcdhγ in the specificity acquired in local neuronal circuits within layer 2/3 could be regulated by the number of cPcdhγ isoforms expressed in PV^+ neurons (Fig10). Although there was no statistically significant difference because of the small number of samples, the number of cPcdhγ isoforms, including C-type isoforms, expressed in PV^+ neurons showed a similar distribution to High- and Low-RPV in that there were many PV^+ neurons with high expression and some with low expression. The reason why the results are not as clear as the distribution in RPV could be caused by the number of detections in RNA patch-seq. In the future, I will need to gather more data from further experiments to make these results more reliable. In order to clarify the differences in the properties of these two types of PV^+ neurons in more detail,

it is necessary to compare their cell morphology, electrical membrane properties, and inhibitory synaptic coupling probability.

Reciprocal connection forms between PV^+ neurons and Pyr neurons in relation to cPcdh isoforms.

This study showed that the reciprocal connection pair had a significantly higher rate of cPcdh isoform match compared to shuffle data. Significant differences were identified only for all cPcdh isoforms and C-type isoforms. The results for all cPcdh isoforms are likely to reflect the results for the C-type. However, the match rate for each of the five isoforms of C-type was almost the same as that of the shuffle data. This suggests that in the C-type, the match of one isoform does not affect reciprocal connections. Interestingly, however, the match rates for the other variable isoforms are not significantly different, but I can observe some isoforms that differ from the trend of match rates in the shuffle data. For example, cPcdhγa2 tends to have a high isoform matching rate for reciprocal pairs ($p=0.0972$). On the other hand, there were several isoforms, such as cPcdhα6, that were expressed to some extent rate in both cells but did not have any matched pairs. These findings suggest that different isoform species could have different roles in synaptogenesis. The reason why I did not see dramatic isoform matches in reciprocal pairs could be related to the samples collected and their numbers.

In this experiment, most of the pairs obtained in RNA-seq were reciprocal connected (20/24 pairs) and could not be compared with one-way connected or no connected pairs. To confirm this result, I need to collect more samples and analyze each connection pattern and its isoform matching rate.

MATERIAL AND METHODS

Animals.

The animal experiments in this study were conducted in accordance with the Osaka University Experimental Regulations (Approval Number: FBS-14-002-1). Mice are kept in a 24-hour cycle with 12 hours of light and 12 hours of dark. All experiments were performed when the mice were 21-26 days old. PV^+ inhibitory neuron-specific *cPcdhγ* deletion mice were generated by crossing PV^+ neuron-specific Cre expressing mice (PV-ires-Cre, B6;129P2-Pvalbtm1(cre)Arbr/J, Jackson Lab, 008069) with *cPcdhgflox* mice (Tarusawa et al., in preparation), in which a *loxP* sequence were inserted before and after the *CR1* exon of the *cPcdhγ* gene (previously generated in our laboratory and shown to cause Cre-dependent loss of cPcdhγ protein). To visualize PV^+ inhibitory neurons, PV-Cre mice and $cPcdhgflox^{PV\text{-}Cre}$ mice were also crossed with Ai14 mice. For conditional KO mice (*flox*-homo*, PV-Cre*-hetero, *Ai14*-homo or hetero), mice without *flox* were used as Control (PV-Cre-hetero, Ai14-homo or hetero).

Electrophysiology

Mice were anesthetized with isoflurane, and transcardially perfused with 5ml ice-cold normal artificial cerebrospinal fluid (ACSF) containing kynurenic acid (126mM NaCl, 3mM KCl, 1.3mM MgSO4, 1.2mM NaH2PO4, 2.4mM CaCl2, 26mM NaHCO3, 10mM Glucose, Kynurenic acid 1mM), saturated with 95% O_2 and 5% CO_2. The brain was removed, and 300 μm thickness acute slices containing primary visual cortex were prepared using a micro slicer. The Slices were allowed to recover at 32 - 34 °C for 1 hour by replacing them in the interface chamber through a normal ACSF oxygenated with 95% O_2 and 5% CO_2. Room temperature normal ACSF oxygenated with CO_2・O_2 mixture gas was flowed at a rate of 2.6 ml/min into the submerged chamber of the upright microscope, where the recording slices were placed at layer 1 of V1 was parallel to the field of view of the camera. The recording glass microelectrodes were made of glass capillaries in a 3-stage pull with a pipette resistance of 5-7 MΩ. All whole-cell patch recordings were recorded from cells at depths greater than 50 μm from the slice surface, within layer 2/3 of the V1 field, under near-infrared differential interference microscopy. PV^+ neurons were recorded from tdTomato-positive cells and depolarizing pulse was induced in current-clamp mode, confirming that the firing pattern was fast-spiking. Pyramidal (Pyr) neurons were recorded from that had a triangle-like shape visually, and after the experiment, biocytin injected into the recording cells was stained, and non-Pyr neurons were excluded from the analysis. The resting membrane potentials (RMP) was recorded immediately after whole-cell patch recordings started. Firing patterns evoked by depolarizing current injections were measured in current-clamp mode. Input resistance were recorded in voltage-clamp mode. In PV^+ neurons firing properties were analyzed first action potential. In these cases, glass electrodes filled with K^+-base solutions (130mM K-gluconate, 8mM

KCl, 10mM HEPES, 1mM MgCl2, 0.6mM EGTA, 10mM Na-phosphocreatine, 3mM MgATP, 0.5mM Na2GTP, 0.2 Biocytin, pH 7.3 adjusted by KOH).

In the simultaneous whole-cell recording of PV^+ neuron - Pyr neuron pairs, whole-cell patches were conducted on PV^+ neurons in layer 2/3 of the primary visual cortex (V1) within the monocular region, and then Pyr neurons within 50 μm of the patch were selected for whole-cell recording. To obtain uEPSC, the recording electrode of PV^+ neuron was filled to K^+-base solutions and the holding potential was set to the reversal potential of the inhibitory postsynaptic currents (-70 mV). To obtain uIPSC, the recording electrode of Pyr neuron was filled to Cs^+-base solutions (130mM Cs-gluconate, 8mM KCl, 10mM HEPES, 1mM MgCl2, 0.6mM EGTwereA, 10mM Na-phosphocreatine, 3mM MgATP, 0.5mM Na2GTP, 0.2 Biocytin, pH 7.3 adjusted by CsOH) and the holding potential was set to the reversal potential of the excitatory postsynaptic currents (0 mV). Pyr neurons were fired twice at 50 ms intervals and PV^+ neurons were fired twice at 100 ms intervals, and the uIPSC and uEPSC for those stimulations were recorded 50 times 2 seconds intervals. Only recordings used that series resistance (Rs: electrical resistance between the recording electrode and the cell membrane) of less than 25 MΩ. After recording, the slices were fixed in 4% PFA in 0.1 M PB 500 μl overnight at 4°C. After fixation, the recording cells were visualized by staining with streptavidin to confirm that the recording was from the target cell type.

Laser photostimulation

The experiment was conducted according to the methods of previous studies (Yoshimura & Callaway, 2005; Ishikawa et al., 2014). Photostimulation was achieved by focal photolysis of RuBi-caged glutamate (TOCRIS; 3574) with 10 ms flashes of blue light (440 nm) from a diode laser. The light was focused on the slices through an X4, 0.16 NA microscope objective and the diameter of the laser was about 20 μm on the slice surface. The cell-attached recording was performed on layer 2/3 Pyr neurons, and the laser intensity was adjusted to fire the recording cells at 1 or 2 stim sites by photostimulation at 5 × 5 sites around the recording cell bodies. The results showed that most of the recorded cells had action potentials at the stim sites within about 100 μm from the center of the cell body. In this study, I recorded EPSCs from cell activation induced by photostimulation received by PV^+ neurons in 2/3. The EPSCs were measured in voltage-clamp mode with the holding potential at -70 mV to isolate EPSCs. Photostimulations were applied quasi-randomly sequence to an 8 × 11 area surrounding the recorded cell, once every 8 seconds.

Single-cell patch sequence

The same method was used as in the previous study (Masuda, in preparation. Before sample collecting, wipe the surfaces of equipment that are frequently touched during the experiment, such as pipet man, electrode puller; workbench, with RNase Zap and DNA-OFF, and then wipe with 70% ethanol to remove RNase. The intracellular fluid used for whole-cell recording was a mixture

of 190 µl Cs^+-base or K^+-base intracellular fluid, 2.5 µl RNase inhibitor (TaKaRa, Recombinant RNase Inhibitor: 2313A) and 10 µl RNase free water. It was prepared just prior to the experiment using a filter tip in a clean bench. A loader tip (Eppendolf, Microloader: 5242956003) was used to fill the glass electrode with 0.5 µl of the above inner solution. After whole-cell recording, the cytoplasm was aspirated into a glass electrode while slowly applying negative pressure, confirming that the size of the recording cell body was reduced using differential interference microscopy. Then, the negative pressure was released and the contents of the electrode were collected by gently folding the tip with the wall of a PCR tube (TaKaRa, 0.2 ml Hi-Tube Dome Cap: NJ200) containing 1.5 µl of Cell Lysis Buffer and applying a small amount of positive pressure. After that, to collect the sample on the wall, centrifugation at 10,000 × g for 1 minute at 4°C, mixing with a vortex mixer for 30 seconds, and centrifugation again at 10,000 × g for 1 minute at 4°C were conducted. The samples were frozen in liquid nitrogen and stored at -80°C after the experiment. The preparation of library DNA was basically performed according to the RamDA-seq protocol (Hayashi et al., 2018). Cell Lysis Buffer of the above composition was used, and the other reaction solution volumes were double the usual protocol. Also, I used 8 tubes and 8 magnets instead of 96 wells. Hisat2 was used as the mapping software. Bigwig format was used for the output, and the sequence reads were visualized using the Integrative Genomics Viewer. I checked the read peaks in the exons, and for samples with reading in the introns, I also confirmed by eye that the peaks were higher in the exons than in the surrounding introns, and that there was read coverage across the bases in the exons. In the case where the boundary of the intron and exon regions was difficult to distinguish, the BAM file was visualized using IGV, and each variable exon was identified based on information such as whether the read of the variable exon protruded from the exon region and whether it was connected to the exon of the constant region, I carefully checked each one. MATLAB (MathWorks) was used to analyze the binarized cPcdh-expressing isoforms.

Analisis

Statistical analysis software GraphPad Prism was used to test for normal distribution and equal variances (D'Agostino-Pearson omnibus normality test), followed by Mann-Whitney test or Welch's t test was conducted. The chi-square, Fisher's exact test, and Kolmogorov-Smirnov test were also performed. The analysis of EPSCs induced by light stimulation was performed using MATLAB in the same way as in previous studies (Yoshimura & Callaway).

REFERENCES

Adachi, H. The role of clustered protocadherin gamma in somatostatin-positive inhibitory neurons in the mouse barrel cortex during early stage of postnatal development. In preparation.

Ariga, R. Gamma-Protocadherins regulate cortical interneuron function. In preparation.

Atallah, B. V., Bruns, W., Carandini, M., & Scanziani, M. (2012). Parvalbumin-expressing interneurons linearly transform cortical responses to visual stimuli. *Neuron*, 73(1), 159-170.

Briggs, F. (2010). Organizing principles of cortical layer 6. *Frontiers in neural circuits*, 4, 3.

Burkhalter, A. H. (2008). Many specialists for suppressing cortical excitation. *Frontiers in neuroscience*, 2, 26.

Carriere, C. H., Wang, W. X., Sing, A. D., Fekete, A., Jones, B. E., Yee, Y., ... & Lefebvre, J. L. (2020). The γ-Protocadherins regulate the survival of GABAergic interneurons during developmental cell death. *Journal of Neuroscience,* 40(45), 8652-8668.

Celio, M. R. (1986). Parvalbumin in most γ-aminobutyric acid-containing neurons of the rat cerebral cortex. *Science*, 231(4741), 995-997.

DeFelipe, J. (1997). Types of neurons, synaptic connections and chemical characteristics of cells immunoreactive for calbindin-D28K, parvalbumin and calretinin in the neocortex. *Journal of chemical neuroanatomy*, 14(1), 1-19.

Defelipe, J., González-Albo, M. C., Del Río, M. R., & Elston, G. N. (1999). Distribution and patterns of connectivity of interneurons containing calbindin, calretinin, and parvalbumin in visual areas of the occipital and temporal lobes of the macaque monkey. *Journal of Comparative Neurology*, 412(3), 515-526.

D'Souza, R. D., Bista, P., Meier, A. M., Ji, W., & Burkhalter, A. (2019). Spatial clustering of inhibition in mouse primary visual cortex. *Neuron*, 104(3), 588-600.

Esumi, S., Kakazu, N., Taguchi, Y., Hirayama, T., Sasaki, A., Hirabayashi, T., ... & Yagi, T. (2005). Monoallelic yet combinatorial expression of variable exons of the protocadherin-α gene cluster in single neurons. *Nature genetics*, 37(2), 171-176.

Gonchar, Y., & Burkhalter, A. (1997). Three distinct families of GABAergic neurons in rat visual cortex. *Cerebral cortex (New York, NY: 1991)*, 7(4), 347-358.

Gouwens, N. W., Sorensen, S. A., Berg, J., Lee, C., Jarsky, T., Ting, J., ... & Koch, C. (2019). Classification of electrophysiological and morphological neuron types in the mouse visual cortex. *Nature neuroscience*, 22(7), 1182-1195.

Haas, I. G., Frank, M., Véron, N., & Kemler, R. (2005). Presenilin-dependent processing and nuclear function of γ-protocadherins. *Journal of Biological Chemistry*, 280(10), 9313-9319.

Hayashi, T., Ozaki, H., Sasagawa, Y., Umeda, M., Danno, H., & Nikaido, I. (2018). Single-cell full-length total RNA sequencing uncovers dynamics of recursive splicing and enhancer RNAs. *Nature communications*, 9(1), 1-16.

Hofer, S. B., Ko, H., Pichler, B., Vogelstein, J., Ros, H., Zeng, H., ... & Mrsic-Flogel, T. D. (2011). Differential connectivity and response dynamics of excitatory and inhibitory neurons in visual cortex. *Nature neuroscience*, 14(8), 1045-1052.

Ishikawa, A. W., Komatsu, Y., & Yoshimura, Y. (2014). Experience-dependent emergence of fine-scale networks in visual cortex. *Journal of Neuroscience*, 34(37), 12576-12586.

Kaneko, R., Kato, H., Kawamura, Y., Esumi, S., Hirayama, T., Hirabayashi, T., & Yagi, T. (2006). Allelic gene regulation of Pcdh-α and Pcdh-γ clusters involving both monoallelic and biallelic expression in single Purkinje cells. *Journal of Biological Chemistry*, 281(41), 30551-30560.

Kawaguchi, Y., & Kubota, Y. (1997). GABAergic cell subtypes and their synaptic connections in rat frontal cortex. *Cerebral cortex (New York, NY: 1991)*, 7(6), 476-486.

Kisvárday, Z. F., & Eysel, U. T. (1993). Functional and structural topography of horizontal inhibitory connections in cat visual cortex. *European Journal of Neuroscience*, 5(12), 1558-1572.

Ko, H., Cossell, L., Baragli, C., Antolik, J., Clopath, C., Hofer, S. B., & Mrsic-Flogel, T. D. (2013). The emergence of functional microcircuits in visual cortex. *Nature*, 496(7443), 96-100.

Kohmura, N., Senzaki, K., Hamada, S., Kai, N., Yasuda, R., Watanabe, M., ... & Yagi, T. (1998). Diversity revealed by a novel family of cadherins expressed in neurons at a synaptic complex. *Neuron*, 20(6), 1137-1151.

Kubota, Y., Karube, F., Nomura, M., & Kawaguchi, Y. (2016). The diversity of cortical inhibitory synapses. *Frontiers in neural circuits*, 10, 27.

Leon, W. R. M., Spatazza, J., Rakela, B., Chatterjee, A., Pande, V., Maniatis, T., ... & Alvarez-Buylla, A. (2020). Clustered gamma-protocadherins regulate cortical interneuron programmed cell death. *Elife*, 9, e55374.

Markram, H., Toledo-Rodriguez, M., Wang, Y., Gupta, A., Silberberg, G., & Wu, C. (2004). Interneurons of the neocortical inhibitory system. *Nature reviews neuroscience*, 5(10), 793-807.

Masuda, H. Patch-RamDA-seq reveals the single-cell gene expression patterns of clustered protocadherins and their relationship with the neural connections and cell lineage. In preparation.

McColgan, P., Joubert, J., Tabrizi, S. J., & Rees, G. (2020). The human motor cortex microcircuit: insights for neurodegenerative disease. *Nature Reviews Neuroscience*, 21(8), 401-415.

Molumby, M. J., Anderson, R. M., Newbold, D. J., Koblesky, N. K., Garrett, A. M., Schreiner, D., ... & Weiner, J. A. (2017). γ-protocadherins interact with neuroligin-1 and negatively regulate dendritic spine morphogenesis. *Cell reports*, 18(11), 2702-2714.

Peng, Y., Barreda Tomas, F. J., Pfeiffer, P., Drangmeister, M., Schreiber, S., Vida, I., & Geiger, J. R. (2021). Spatially structured inhibition defined by polarized parvalbumin interneuron axons promotes head direction tuning. *Science Advances*, 7(25), eabg4693.

Reiss, K., Maretzky, T., Haas, I. G., Schulte, M., Ludwig, A., Frank, M., & Saftig, P. (2006). Regulated ADAM10-dependent ectodomain shedding of γ-protocadherin C3 modulates cell-cell adhesion. *Journal of Biological Chemistry*, 281(31), 21735-21744.

Runyan, C. A., & Sur, M. (2013). Response selectivity is correlated to dendritic structure in parvalbumin-expressing inhibitory neurons in visual cortex. *Journal of Neuroscience*, 33(28), 11724-11733.

Schreiner, D., & Weiner, J. A. (2010). Combinatorial homophilic interaction between γ-protocadherin multimers greatly expands the molecular diversity of cell adhesion. *Proceedings of the National Academy of Sciences*, 107(33), 14893-14898.

Shipp, S. (2007). Structure and function of the cerebral cortex. *Current Biology*, 17(12), R443-R449.

Southwell, D. G., Paredes, M. F., Galvao, R. P., Jones, D. L., Froemke, R. C., Sebe, J. Y., ... & Alvarez-Buylla, A. (2012). Intrinsically determined cell death of developing cortical interneurons. *Nature*, 491(7422), 109-113.

Steffen, D. M., Ferri, S. L., Marcucci, C. G., Blocklinger, K. L., Molumby, M. J., Abel, T., & Weiner, J. A. (2021). The γ-protocadherins interact physically and functionally with neuroligin-2 to negatively regulate inhibitory synapse density and are required for normal social interaction. *Molecular neurobiology*, 58(6), 2574-2589.

Südhof, T. C. (2008). Neuroligins and neurexins link synaptic function to cognitive disease. *Nature*, 455(7215), 903-911.

Tasic, B., Nabholz, C. E., Baldwin, K. K., Kim, Y., Rueckert, E. H., Ribich, S. A., ... & Maniatis, T. (2002). Promoter choice determines splice site selection in protocadherin α and γ pre-mRNA splicing. *Molecular cell*, 10(1), 21-33.

Tarusawa, E., Sanbo, M., Okayama, A., Miyashita, T., Kitsukawa, T., Hirayama, T., ... & Yoshimura, Y. (2016). Establishment of high reciprocal connectivity between clonal cortical neurons is regulated by the Dnmt3b DNA methyltransferase and clustered protocadherins. *BMC biology*, 14(1), 1-19.

Thu, C. A., Chen, W. V., Rubinstein, R., Chevee, M., Wolcott, H. N., Felsovalyi, K. O., ... & Maniatis, T. (2014). Single-cell identity generated by combinatorial homophilic interactions between α, β, and γ protocadherins. *Cell*, 158(5), 1045-1059.

Wang, X., Su, H., & Bradley, A. (2002). Molecular mechanisms governing Pcdh-γ gene expression: Evidence for a multiple promoter and cis-alternative splicing model. *Genes & development*, 16(15), 1890-1905.

Wonders, C. P., & Anderson, S. A. (2006). The origin and specification of cortical interneurons. *Nature Reviews Neuroscience*, 7(9), 687-696.

Wong, F. K., Bercsenyi, K., Sreenivasan, V., Portalés, A., Fernández-Otero, M., & Marín, O. (2018). Pyramidal cell regulation of interneuron survival sculpts cortical networks. *Nature*, 557(7707), 668-673.

Wu, Q., & Maniatis, T. (1999). A striking organization of a large family of human neural cadherin-like cell adhesion genes. *Cell*, 97(6), 779-790.

Wu, Q., Zhang, T., Cheng, J. F., Kim, Y., Grimwood, J., Schmutz, J., ... & Maniatis, T. (2001). Comparative DNA sequence analysis of mouse and human protocadherin gene clusters. *Genome research*, 11(3), 389-404.

Yagi, T., & Takeichi, M. (2000). Cadherin superfamily genes: functions, genomic organization, and neurologic diversity. *Genes & development*, 14(10), 1169-1180.

Yizhar, O., Fenno, L. E., Prigge, M., Schneider, F., Davidson, T. J., O'shea, D. J., ... & Deisseroth, K. (2011). Neocortical excitation/inhibition balance in information processing and social dysfunction. *Nature*, 477(7363), 171-178.

Yoshimura, Y., & Callaway, E. M. (2005). Fine-scale specificity of cortical networks depends on inhibitory cell type and connectivity. *Nature neuroscience*, 8(11), 1552-1559.

Yu, Y. C., Bultje, R. S., Wang, X., & Shi, S. H. (2009). Specific synapses develop preferentially among sister excitatory neurons in the neocortex. *Nature*, 458(7237), 501-504.

Yu, Y. C., He, S., Chen, S., Fu, Y., Brown, K. N., Yao, X. H., ... & Shi, S. H. (2012). Preferential electrical coupling regulates neocortical lineage-dependent microcircuit assembly. *Nature*, 486(7401), 113-117.

Znamenskiy, P., Kim, M. H., Muir, D. R., Iacaruso, M. F., Hofer, S. B., & Mrsic-Flogel, T. D. (2018). Functional selectivity and specific connectivity of inhibitory neurons in primary visual cortex. *Biorxiv*, 294835.

ACKNOWLEDGMENTS

I would like to express my sincere gratitude to Professor Yagi and Assistant Professor Tarusawa of the Kokoro Laboratory, Graduate School of Frontier Biosciences, Osaka University, for their enthusiastic support and guidance throughout the course of this study. I have had the support and encouragement of the staff of this laboratory for their appropriate technical advice. Professor Kitazawa and Professor Yamamoto of the same Graduate School, and Professor Okamoto of the same university give insightful comments and suggestions. Professor Yoshimura of the Institute of Physiology gives me constructive comments and warm encouragement. I thank Prof. Nikaido, Dr. Hayashi, and Dr. Yoshimura at RIKEN for their great technical contributions to RNA-seq. Lastly, I would like to thank my peer, Mr. Hoshino, for a very meaningful discussion.

ACCOMPLISHMENT

国内学会・シンポジウム等における発表

・ポスター発表 （査読あり）

1. 河村菜々実，足澤悦子，八木健
   “Role of clustered protocadherin gamma for the specific synaptic connections between excitatory and parvalbumin-positive inhibitory neurons in the mouse visual cortex”,
   第 41 回日本神経科学大会, 2018. 7. 26 – 7. 29

2. 河村菜々実，足澤悦子，吉村由美子，八木健
   「クラスター型プロトカドヘリンガンマがマウス大脳皮質視覚野における興奮性細胞とパルブアルブミン陽性細胞間の特異的シナプス結合形成に与える影響」,
   第 41 回日本分子生物学会年会, 2018. 11. 28 – 11. 30

3. 河村菜々実，足澤悦子，吉村由美子，八木健
   “Classification of parvalbumin-positive inhibitory neurons by a difference of local microcircuits and the influence of deletion of clustered protocadherin gamma in the mouse visual cortex”,
   第 42 回日本神経科学大会, 2019. 7. 25 – 7. 28

4. 河村菜々実，足澤悦子，吉村由美子，八木健
   “Deletion of clustered protocadherin gamma caused abnormality of pyramidal neuron - parvalbumin-positive inhibitory neuron connectivity in mouse visual cortex”,
   第 43 回日本神経科学大会, 2020. 7. 29 – 8. 1

・ポスター発表 （査読なし）

1. 河村菜々実，足澤悦子，八木健
   「マウス大脳皮質視覚野において興奮性ニューロンとパルブアルブミンポジティブ抑制性ニューロン間の特異的なシナプス結合におけるクラスター型プロトカドヘリンガンマの役割」,
   生理学研究会　情動研究会, 2018. 9. 18 – 9. 19

その他

・研究費採択状況

1. 特別研究員奨励費　DC2・生物系科学　神経機能学関連
   河村菜々実（代表者）
   「マウス大脳皮質視覚野における微小神経回路の 形成メカニズムと機能的意義の解明」,
   2021. 4. 28 – 2023. 3. 31, 直接経費 800,000 円, 2021 年度